

# Quasi-static and impact perforation of polymer-metal bi-layer plates by a blunt indenter

I. Mohagheghian<sup>a,b</sup>, G.J. McShane<sup>b,\*</sup>, W.J. Stronge<sup>b</sup>

<sup>a</sup> *Department of Mechanical Engineering Sciences, University of Surrey, Guildford,  
GU2 7XH, UK*

<sup>b</sup> *Department of Engineering, University of Cambridge, Trumpington Street,  
Cambridge CB2 1PZ, UK*

*\*Corresponding authors.*

*Tel: +44 1223 332635, Fax: +44 1223 332662, Email: gjm31@cam.ac.uk*

## Abstract

The use of polymer layers to alter the impact response of metallic plates has emerged recently as an effective and economical means to enhance perforation resistance. However, the function of the polymer in such laminate systems remains unclear. In this investigation we aim to identify, through systematic experiments, the influence of a polymer layer on the perforation mechanisms and energy absorption of laminated plates. In particular, we consider the combination of a polymer with a thin metallic plate in a bi-layer configuration, subjected to either quasi-static or impact loading by a blunt indenter. Bi-layers are investigated which comprise an aluminium alloy layer (6082-T6) and a polyethylene layer (LDPE, HDPE and UHMWPE). It is found that the energy required to perforate the bi-layer plate can significantly exceed that of the bare metallic substrate (showing the potential for polymer coatings as an effective retro-fit solution) when the polymer is on the impacted face. Furthermore, bi-layer configurations are also shown to outperform the equivalent mass of monolithic metal if the correct thickness ratio of polymer and metal is selected. The effectiveness of a polymer layer

in enhancing perforation energy is connected to its large ductility, allowing extensive deformation of the polymer under the indenter, which in turn suppresses plugging and diffuses plastic deformation in the metal layer. In this way the energy absorbed by the metal layer can be maximised. The thickness of the polymer layer is found to be a crucial parameter in maximising the effectiveness of the bi-layer target. An optimum polymer thickness is observed which maximises energy absorption per unit mass of bi-layer target (for a fixed substrate thickness). The synergy between metal and polymer layers also depends on the polymer type and the rate of loading. A polymer with high strain hardening performs best under impact conditions. However, under quasi-static loading, the bi-layer performance is less sensitive to the yield strength and strain hardening of the polymer.

*Keywords: polymer-metal bi-layer, impact, perforation, blunt indenter*

## **1. Introduction**

Enhancing the impact perforation resistance of materials at minimum weight is of value in applications such as lightweight vehicle construction and materials for security and defence. Layered materials, of either similar or dissimilar properties, have been investigated as a more effective alternative to monolithic plates of the same mass. Recently, attention has been given to the use of polymer layers to enhance the impact resistance of metallic plates. This has practical advantages: elastomers such as polyurea can be easily and economically applied to a wide variety of surfaces as a retro-fit coating. Initial results indicate promising performance for polymer-metal layered structures [1,2]. However, the mechanisms responsible for enhancing the performance are not clearly understood. In this investigation, we aim to study systematically the influence of a polymer layer on the quasi-static and impact perforation of thin metallic

plates, with targets having a total areal density up to about  $10 \text{ kg m}^{-2}$ . This range of target mass has practical significance for understanding the protection of lightweight and thin-walled structural components, either from a retro-fit perspective (i.e. adding the polymer for reinforcement) or for impact resilient design. Furthermore, we focus on indenters and projectiles with a blunt nose-shape (i.e. flat-nosed circular cylinders). This is an idealised geometry, but provides useful insights into the target response to sharp-edged projectiles such as those generated by the fragmentation of an explosive device. We first briefly review previous work on the impact perforation of laminates, including polymer-metal laminates.

### *1.1 Impact response of metallic laminates*

Layering of metallic plates has been investigated as a strategy for enhancing impact perforation resistance. However, a consensus has not been reached about the effectiveness of layering for single-material systems. The approach has its basis in the observation that when a thick metallic plate is struck by a projectile the deformation will be highly localised (at the projectile perimeter in the case of blunt projectile), whereas a thinner plate (and therefore a stack of thinner plates for heavier structures) achieves a contribution to energy absorption through extensive tensile stretching [3]. Some studies indicate that a monolithic plate is superior to the equivalent mass layered system [4–6], while contrary results have also been reported [7–9]. It appears that the effectiveness of layering depends on many parameters such as nose shape of the projectile [8,9], the number of layers [10], the ratio of the thicknesses of the layers [5,11,12] and the total thickness of the target [11,13,14]. Recently, it has been shown that using materials with dissimilar properties in metallic laminates can provide enhanced impact energy absorption. In a numerical investigation, Teng et al. [15] show

that for low velocity impacts by blunt or conical projectiles, bi-layer metallic laminates absorb more energy than monolithic plates of the same mass if a more ductile metal is used in front (the impacted layer) with a higher strength, lower ductility metal behind. Flores-Johnson et al. [16] also show that using dissimilar materials in different layers in a metallic laminate can be superior to a single material configuration with the same mass. Their results suggest that a thin aluminium plate backed by a thick steel plate can deliver the best energy absorption. In a theoretical analysis of penetration of a layered target by a rigid projectile, Ben-Dor et al. [17,18] suggest that the ballistic limit is greatest if the plates are arranged with those having the smallest ratio of strength to density placed in front (i.e. nearest the impact surface). While these investigations reveal the potential benefits of combining layers with contrasting mechanical properties, the impact response of polymers differs greatly from that of metals, and so they do not provide a complete insight into the performance of polymer layers for impact mitigation.

### *1.2 Impact response of polymer-metal laminates*

An early investigation into polymer-metal laminates was conducted by Radin and Goldsmith [4], comparing the combination of polycarbonate and aluminium alloy (2024-O) plates with equal mass monolithic metal and polymer plates under projectile impact. Although the response of monolithic aluminium and polycarbonate plates were investigated for both blunt and conical nose projectiles, all of the tests performed on the bi-layer configuration were with the conical projectile. Their results indicated that for the same mass per unit area, a bi-layer with the metal layer facing the conical projectile had a ballistic limit above that of monolithic metal, but below that of monolithic polycarbonate. The polycarbonate layer appeared to alter the failure mode in the metal

layer when these materials were combined in a laminate configuration. Low-velocity drop-weight impact tests were conducted by Liu and Liaw [19] on PMMA-aluminium bi-layers with an epoxy adhesive interface. In contrast to [4], their experiments showed that the impact damage (including delamination, and fracture of the polymer) is more severe when the aluminium plate is located on the impacted face. The impact response of an elastomer-steel laminate was investigated by Roland et al. [2]. They considered a variety of elastomers backed by thick High Hard Steel (HHS) plates, and concluded that the glass transition of the polymer is a key parameter. They argue that the greatest improvement in the ballistic limit is achieved for polymers that undergo an impact-induced glass transition, due to the increase in viscoelastic dissipation associated with the transition from rubbery to glassy behaviour. However, the results show a modest (~10%) variation in performance for a wide range of glass transition temperatures, and so, as pointed out by these authors, there are likely to be other significant parameters. Indeed, the importance of polymer layer thickness also emerges from this study: a thin polymer coating can produce a significant increase in energy absorption, yet further increases in thickness have only a small effect. Roland et al. [2] also investigated the effect of the attachment method between the steel and the polyurea on the ballistic perforation. Two methods were considered: i) attachment using mechanical fasteners (i.e. screws) and ii) attachment using adhesives. No measurable difference in the ballistic limit was observed between the two methods. The role of polymer thicknesses was investigated further by Roland et al. [20], impacting polyurea coated metallic plates with a fragment simulating projectile. Again, energy absorption appears more sensitive to the polymer thickness than the chosen polymer type. It is further shown that it is preferable to position the polymer on the impacted face. Xue et al. [21] conducted a series of numerical calculations on steel plates backed by a polyurea coating impacted

by blunt and conical projectiles. The simulations were compared with the experimental results of Mock et al. [1]. It was found that a polyurea backing is more effective for the conical projectile than the blunt projectile. They suggest that, for conical projectiles, the energy absorption in the metal layer is increased due to the polymer retarding the onset of fracture in the steel plate. However, for the blunt projectile, the polyurea backing decreases the energy absorbed by the steel layer, with an overall increase in energy absorption accounted for by stretching of the polyurea.

Polymer layers used in conjunction with a metallic substrate therefore appear to show promise for enhancing perforation resistance. However, the precise function of the polymer layer in altering the dissipation of energy during the impact, and hence the optimal choice of polymer type and thickness for a particular metallic substrate and impact threat, remains unclear. The goal of the current investigation is to address these issues for one impact scenario: the impact of thin metallic plates by a non-deforming blunt projectile. We support the impact results with quasi-static puncture experiments to gain clearer insights into the mechanisms of energy dissipation and the effect of the polymer layer throughout the perforation process.

### *1.3 Outline of the current investigation*

This paper focuses on bi-layer laminates with one metal and one polymer layer (in addition to monolithic plates of either material for comparison). This laminate is particularly relevant to inform the design of retro-fit polymer coatings that aim to mitigate impact damage. By understanding the interactions between the two layers and the mechanisms of energy absorption, we gain insights into optimisation of the laminate for perforation resistance. To ensure controllable, repeatable layer properties and thicknesses, we opt for aluminium alloy 6082 for the metallic layer and extruded

polyethylene sheets of various types for the polymer layer (providing a variety of mechanical properties, while maintaining other parameters, such as polymer density and glass transition temperature, approximately constant). In this study, no adhesive is used between the polymer and metal layers. We acknowledge that an adhesive may be necessary in practice, e.g. for large-scale application of polymer coatings. However, in the current investigation we opt for a simplified arrangement, with the layers in frictional contact only. As will be discussed subsequently, the key deformation mechanisms that we identify are not expected to be sensitive to the interface bonding conditions. This is also consistent with the findings of Roland et al. [2], that the regimes of response under consideration are largely independent of interface strength. Removing this additional variable allows the number of experimental parameters in this investigation to be better controlled.

The paper is structured as follows. The quasi-static perforation behaviour is first investigated, gaining insight into the stages of deformation and failure in the absence of significant inertia and strain-rate effects (Section 2). This research indicates that a polymer layer placed between the indenter and the metallic layer can enhance energy absorption, not directly through dissipation within the polymer itself, but indirectly, by altering the mode of failure, and hence plastic dissipation, in the metal layer. This is pursued further in Section 3 by determining how this effect varies as the polymer layer thickness is changed. This study shows clearly that the function of the polymer in the bi-layer configuration is to alter the effective nose shape of the indenter. An optimal polymer-metal thickness ratio emerges. To explain this observation, in Section 4, the effect is analysed in detail, by comparing the bi-layer results with a series of experiments designed to simulate the same effect, but through direct variation of the indenter tip geometry. These indicate that a specific effective tip geometry, intermediate

between blunt and hemi-spherical, maximises plastic dissipation in the metal layer, and induces a failure mechanism that matches the optimum bi-layer cases. In Section 5, the impact perforation of monolithic and bi-layer plates is investigated using a gas gun apparatus, with impact velocities up to  $180 \text{ m s}^{-1}$ . Similar behaviour is observed in the quasi-static case, with a polymer layer facing the projectile resulting in a significant increase in the perforation energy. In Section 6, the influence of the mechanical properties of the polymer layer on the effective nose shape change and the perforation resistance of a laminate are investigated. By comparison with metallic targets of the same mass, the significant performance advantage of the bi-layer configuration is demonstrated, both quasi-statically and dynamically. In Section 7, alternative energy absorption mechanisms proposed in the literature are assessed for the current material combination. Finally, concluding remarks are given in Section 8.

## **2. Quasi-static perforation of a bi-layer laminate**

First consider the quasi-static perforation response of a single polymer-metal bi-layer plate configuration in comparison with monolithic plates of the constituent materials. The objective is to understand the effect of layering on the deformation, fracture development, energy absorption, and in particular whether the arrangement of the layers is significant for this material system, as was shown to be the case by Teng et al. [15] for metallic laminates. A quasi-static perforation test allows the physical mechanisms of deformation and failure to be studied more easily, in the absence of inertia and strain-rate effects. As will be shown subsequently, the quasi-static tests provide relevant insights into the impact response.

### *2.1 Test configuration*

The test specimens used in this investigation consisted of flat plates with a circular target area fully clamped around the edge at a radius  $R = 50$  mm. The boundary condition was provided by a circular steel clamping ring with inner diameter 100 mm, as shown in Fig. 1. Twelve M4 bolts were used to fasten the clamping ring through clearance holes in the test specimen (a square plate of side length 130 mm) to a supporting plate. The indenter was a solid circular cylinder, referred to subsequently as blunt tipped, with a diameter of 12.5 mm. The ratio of indenter to plate radius was therefore  $R_i / R = 0.125$ . The indenter was machined from mild steel, and underwent no plastic deformation during the indentation experiments.

The bi-layer test specimen consisted of one metal and one polymer layer of approximately equal mass. The metal layer was aluminium alloy 6082-T6 ( $\rho = 2700$  kg m<sup>-3</sup>) with thickness  $h_m = 1$  mm, and mass per unit area  $m = 2.70$  kg m<sup>-2</sup>. The polymer layer was extruded low density polyethylene (LDPE,  $\rho = 930$  kg m<sup>-3</sup>) sheet with thickness  $h_p = 3$  mm, and mass per unit area  $m = 2.79$  kg m<sup>-2</sup>. In order to characterise each material, tensile tests were performed using an Instron screw driven test machine on dog-bone specimens machined with dimensions matching the standard ASTM-D638 for the polymer and ASTM-E8 for the metal. Nominal tensile stress-strain curves are plotted in Fig. 2 for each material. Nominal stress measurements were obtained from the test machine load cell readings. Nominal strain was obtained from the cross-head displacement for the polymer specimens. A laser extensometer was used for the metallic specimens. (Note that nominal stress and strain are used here as the onset of deformation localisation in the polymer specimens means that true stress and strain cannot be reliably calculated from the experimental data.) The 6082-T6 has a yield strength of approximately 300 MPa, and fails at around 16% nominal tensile strain (Fig. 2a). The LDPE has a yield strength of around 12 MPa, and undergoes limited strain

hardening prior to fracture at a nominal strain of approximately 700% (Fig. 2b). In the bi-layer configuration, the polymer and metal plates are clamped together in frictional contact only; no adhesive is used between the layers.

The quasi-static perforation experiments were performed using an Instron screw driven test machine. The blunt indenter was mounted to the load cell on the cross-head of the machine with the specimen and clamping plate supported beneath. The load cell was used to record the indentation force, and the cross-head displacement gave the indentation distance (it was confirmed that cross-head compliance has a negligible influence on the measurements for the specimens tested here). All of the indentation tests were conducted at a rate of  $1 \text{ mm min}^{-1}$ . The tests were stopped after the indenter had fully perforated all layers.

## *2.2 Phases of deformation: monolithic plates*

The quasi-static result for a monolithic aluminium alloy (6082-T6) plate with thickness  $h_m = 1 \text{ mm}$  is shown in Fig. 3a. The response can be divided into two phases: before (phase 1) and after (phase 2) fracture of the metal. Phase 1 consists of elastic-plastic bending and stretching of the plate. This can be further subdivided: in phase 1a, the response is non-linear, and corresponds to elastic and plastic bending of the plate, accompanied by some local plastic deformation around the indenter tip. In phase 1b the response is approximately linear, and is dominated by plastic membrane stretching. Later in phase 1b localisation of deformation at the edge of the indenter leads to a deviation from the linear trend. At the end of phase 1, the plate fractures around the periphery of the contact area. The failure mode for a blunt indenter pressing against a monolithic Al alloy plate is shown in Fig. 4a: a disc is cut by the indenter through local failure at the perimeter ('plugging'). Further resistance to indentation in phase 2, after

fracture of the metal plate, is due to further bending and crack propagation where the disc cut by the indenter remains hinged to the rest of the plate at one point on its perimeter: Fig. 4a.

The linear trend during phase 1b has been observed previously for both thin and thick metallic plates [22–24]. The analysis of Oant and Haythornthwaite [22], which considers only the membrane stretching deformation of a rigid-ideally plastic circular plate loaded over a central patch, predicts a linear force-deflection response with gradient proportional to the material yield strength. Simonsen and Lauridsen [25] derive a semi-analytical model for the indentation of a circular plate by a spherical indenter, accounting for strain hardening of the material (via a power law relationship). They showed that, in comparison with an ideally plastic model, strain hardening increases the gradient of the force-deflection response during phase 1b, although the response remains approximately linear in this phase.

The indentation response of a monolithic LDPE plate of thickness  $h_p = 3$  mm is compared with the monolithic metal plate in Fig. 3b. Although the plot of indenter force  $F$  versus displacement  $u_i$  has a similar overall shape to that of the metal case, the lower yield strength of the polymer reduces significantly the slope during plastic membrane stretching (phase 1b). The higher ductility of the polymer also delays failure to a larger depth of indentation. As a result, the total energy absorbed during perforation of the plate is comparable with that of the monolithic metal plate (9.5 J for the polymer compared to 13.5 J for the metal). Here, we define energy absorption as the work done  $W$  by the indenting force

$$W = \int F du_i . \quad (1)$$

The failed polymer plate is shown in Fig. 4b. Failure is again by plugging, similar to that of the monolithic metal, although recovery of the large elastic strains in the plate results in a final hole diameter that is somewhat smaller than the indenter diameter.

### 2.3 Indentation of LDPE / aluminium alloy bi-layers

Two LDPE-aluminium alloy bi-layer configurations were considered: (i) metal layer in front (i.e. in contact with the indenter) and (ii) polymer layer in front. In both cases the metal layer thickness  $h_m = 1$  mm and the polymer layer thickness  $h_p = 3$  mm. The indenter force versus displacement results for both cases are shown in Fig. 3b. Considering first the case with the metal layer in contact with the indenter, the response initially follows that of the monolithic metal. Upon failure of the metal layer at  $u_i \approx 6$  mm, the response then follows closely that of the monolithic polymer. There therefore appears to be no synergy between the layers in this configuration: the indentation response is close to the superposition of the two independent monolithic results. The failure mode is shown in Fig. 4c (the contact surface is shown). The metal and polymer layers both fail by plugging, similar to their monolithic equivalents.

Consider now the case with the polymer layer in contact with the indenter (marked ‘polymer in front’ in Fig. 3b). For this configuration, the gradient of the indenter force-displacement response up to the first drop in load is smaller than that for the monolithic metal case. However, the onset of failure in the metal layer (corresponding to the first load drop in Fig. 3b) is significantly delayed. The total energy required to perforate the bi-layer plate with the polymer in front (59.0 J) is therefore significantly greater than either that for the monolithic metal case (13.5 J) or the bi-layer configuration with the metal as the contacted layer (28.8 J). The deformed plate at the point of metal fracture is shown in Fig. 4d (showing the distal surface). At this point the polymer has yet to

fracture. We note that the mode of failure of the metal layer is significantly different from that of the bi-layer with metal as the contact surface (Fig. 4c). Instead of fracturing at the perimeter of the indenter, a crack initiates nearer the centre of the plate. The plate also shows significantly more plastic deformation ('dishing') around the indenter than the other configurations. The increase in phase 1 energy absorption can be attributed to this dishing deformation. If loading continues to failure of the LDPE layer, the deformed plate is as shown in Fig. 4e. Three unequally-sized petals form, which undergo further bending and crack growth with increasing indenter displacement. For this configuration the significant energy absorption in phase 2 can be attributed to this petal deformation. Clearly, for the bi-layer configuration with the polymer as the contacted surface, there is a strong synergy between the layers. The change in the failure mode of the metal layer, from plugging to more extensive dishing and tensile failure, is similar to that observed when a metallic plate is loaded by a round-tipped instead of a blunt-tipped indenter.

### **3. The role of the polymer thickness on the effective nose shape change**

We next present a series of quasi-static indentation experiments in which the thickness of the polymer layer is varied (with the metallic substrate unchanged). By progressively increasing the polymer thickness, from zero to a thickness of the order of the projectile radius, we aim to clarify the connection between the effective nose shape change, the mechanism of failure and the perforation energy

The constituent materials are again LDPE and aluminium alloy 6082-T6. We consider bi-layer plates with the polymer facing the indenter (the configuration for which the effective nose shape change occurred). The thickness of the metal layer  $h_m = 1$  mm is

held fixed. Four values of polymer thickness were considered,  $h_p = 1.6, 3.0, 4.5$  and  $5.9$  mm (i.e.  $h_p / R_i = 0.26-0.94$ ). To measure local indentation of the polymer layer, two separate displacement measurements were taken: (i) the crosshead displacement (i.e. the displacement of the indenter)  $u_i$ , and (ii) the displacement of the back (distal) face of the metal layer  $u_B$ , measured using an LVDT displacement transducer in contact with the centre of the plate.

The quasi-static indentation results are plotted in Fig. 5 for a monolithic aluminium alloy (6082-T6) plate of thickness  $h_m = 1$  mm, i.e. the bare substrate, and bi-layer plates with  $h_m = 1$  mm and increasing polymer layer thickness  $h_p$ . Fig. 5a shows the variation in indenter force  $F$  with the indenter displacement  $u_i$ . For all polymer thicknesses, the polymer layer increases the compliance during phase 1 (i.e. reduces  $\partial F / \partial u_i$ ), but also substantially delays the onset of failure. The net result is an increase in total energy absorption, Eq. (1), with increasing polymer thickness, shown in Fig. 5b.

To understand in more detail what is occurring as the polymer thickness is increased, the perforation energy is decomposed into two contributions in Fig. 5b: the energy absorbed before failure of the metal (phase 1) and after metal failure (phase 2). This shows that the phase 1 energy absorption, which is predominantly due to dishing deformation in the metal layer (Fig. 4), reaches a plateau at  $h_p \approx 3$  mm. Further insight into this plateau can be gained from Fig. 5c, a comparison of the displacements at the onset of metal fracture of the indenter ( $u_{if}$ ) and the distal face of the metal layer ( $u_{Bf}$ ). The latter, obtained from the LVDT measurements, gives an indication of the degree of dishing deformation in the metal layer. Increasing  $h_p$  initially increases  $u_{Bf}$ , but it reaches a maximum when  $h_p = 3$  mm. Profilometry of the distal face of the metal layer confirmed a reduction in dishing deformation for  $h_p > 3$  mm. The amount of local polymer deformation in phase 1 (represented by  $(u_{if} - u_{Bf})$  in Fig. 5c) continues to

353 increase for  $h_p > 3$  mm, contributing to the indentation work. However, due to the  
 354 lower strength of the polymer layer, this is a less effective dissipation mechanism than  
 355 metal layer plasticity. The consequence of this can be seen if the total energy absorption  
 356 is expressed *per unit mass* of plate

$$\bar{W} = \frac{W}{\rho_m h_m + \rho_p h_p}, \quad (2)$$

357 which is plotted in Fig. 5b, for comparison.  $\bar{W}$  is a maximum at  $h_p = 3$  mm, where the  
 358 dishing deformation in the metal layer is a maximum. This result indicates that there is  
 359 a critical polymer thickness that maximises the performance of the laminate.

360 The critical polymer thickness in Fig. 5 can be explained in terms of an effective nose  
 361 shape change, evident by inspecting the evolution of the mode of failure of the plate as  
 362  $h_p$  is increased. Photographs of the rear (distal) face of the monolithic and bi-layer plates  
 363 at the onset of fracture in the metal are shown in Fig. 6. As the polymer thickness  
 364 increases, there is a progressive transition in the mode of failure, with the fracture  
 365 initiation point moving from the edge of the indenter to the centre of the plate. This  
 366 effective nose shape change is further evident in the polymer ‘caps’, detached from the  
 367 polymer plate at the tip of the indenter, and subsequently retrieved for inspection  
 368 (shown in Fig. 6). Although the recovered shape of each ‘cap’ will not match that under  
 369 load (due to elastic recovery), the influence of the polymer layer thickness on altering  
 370 the tip geometry is evident. This phenomenon, and its responsibility for the optimum  
 371 bi-layer configuration, will be analysed further in Section 4.

372 We note that the result above has been obtained for a particular value of the indenter  
 373 radius, i.e. the non-dimensional group  $R_i / R$  is held constant. In this investigation, a  
 374 small value of  $R_i / R = 0.125$  is chosen, for which the metal plate deforms predominately

in a tensile membrane mode. Increasing  $R_i / R$  can lead to a change in the deformation mode of the metal layer and, consequently, may alter the mechanisms of interaction between the layers. The optimum value of the polymer thickness may then change.

### *3.1 Substrate thickness*

In order to assess the sensitivity of the indentation phenomena described above to the metal layer thickness, the experiments were repeated with the aluminium alloy substrate thickness increased to  $h_m = 2$  mm. Again, we consider bi-layer plates with polymer thicknesses  $h_p = 1.6, 3.0, 4.5$  and  $5.9$  mm. In all cases, the metallic layer is the same aluminium alloy 6082-T6 and the polymer is LDPE, placed on the front (contact) surface.

The quasi-static results for the  $h_m = 2$  mm bi-layers are given in Fig. 7, and compared with the  $h_m = 1$  mm case. The deformed specimens are shown in Fig. 6. The same failure mode transition from plugging failure to dishing and tensile failure as the polymer layer thickness is increased occurs for the thicker substrate. The increase in perforation energy achieved by adding a particular polymer thickness is, however, larger for the thicker substrate (Fig. 7), due to the additional work done in plastic deformation of the metal later.

## **4. Analysis of the effective indenter tip geometry change**

To better understand the indenter nose shape change effect described in Section 3, a series of experiments was performed on monolithic metallic plates loaded by a range of systematically varied indenter tip geometries. The plates were identical to those used in the bi-layer experiments (aluminium alloy 6082-T6,  $h_m = 1$  mm). The geometries of the

indenter are shown in Fig. 8. The geometry was modified from blunt to hemi-spherical in two ways: (i) by increasing the chamfer radius at corner of the indenter, and (ii) by maintaining the centre of curvature of the tip on the indenter axis and reducing the tip radius (as in Corran et al., 1983b). Although the indenters are non-deformable, the relationship between tip shape and plate failure mode provides insights that support the interpretation of the bi-layer results.

The indenter force  $F$  versus indenter displacement  $u_i$  is shown in Fig. 9a for indenters with four chamfer radii:  $R_c = 0, 1.5, 4.5$  and  $6.25$  mm (the latter being equal to  $R_i$ ). Results are given in Fig. 9b for indenters with four tip radii,  $R_f = 7.5, 9.0, 12.0$  and  $30.0$  mm, in addition to the hemi-spherical and blunt cases, corresponding to  $R_f = 6.25$  mm and  $R_f = \infty$  respectively. Increasing  $R_c/R_i$  reduces the slope  $\partial F/\partial u_i$  within the membrane stretching phase (phase 1). However, the indenter displacement at fracture ( $u_{if}$ ) increases with increasing  $R_c/R_i$ , resulting in an overall increase in the perforation energy (Fig. 9c). A similar reduction in slope can be seen in Fig. 9b with increasing  $R_i/R_f$ . However, the indenter displacement at fracture  $u_{if}$  increases initially (up to  $R_i/R_f = 0.69$ ) and then decreases. This results in a maximum in the perforation energy, Fig. 9c. The deformed plates at the point of fracture are shown in Fig. 10 for all indenter tip geometries. Increasing either  $R_c/R_i$  or  $R_i/R_f$  from 0 to 1 results in a transition from failure at the perimeter of the indenter to failure at the centre of the plate. The transition occurs over a narrow range of  $R_i/R_f$ , between 0.53 and 0.69, which also corresponds to the peak in perforation energy in Fig. 9c. However, the transition in failure mode occurs more gradually when increasing  $R_c/R_i$ , with fracture always occurring in the region of contact with the chamfer. Increasing the polymer layer thickness  $h_p$  for bi-layer targets with the polymer facing the indenter therefore leads to a variation in

423 response (in terms of both perforation energy and failure mode transition of the metallic  
424 substrate) that is more consistent with the polymer layer increasing  $R_i/R_f$ .

425 A comparison is made in Fig. 11 between the quasi-static indentation response, using a  
426 blunt indenter, of three bi-layers ( $h_p = 1.5, 3$  and  $6$  mm) with that of a monolithic metal  
427 plate loaded by indenters with different  $R_f$ . In the bi-layer case, the back face deflection  
428 of the metal layer ( $u_B$ ) is used (the indenter displacement includes a contribution from  
429 the polymer compliance). For the monolithic metallic plate, indenter displacement and  
430 back face displacement are identical to within  $0.2$  mm, and so indenter displacement is  
431 used, for convenience.

432 In Fig. 11a, the indentation response of the bi-layer with  $h_p = 1.5$  mm is compared with  
433 that of monolithic metal plates loaded by three different indenter nose shapes. The  
434 response of the bi-layer initially follows that of the monolithic metal loaded by a blunt  
435 indenter, but deviates at larger indenter displacements. Fracture occurs at a  
436 displacement of approximately  $10.5$  mm, which is closest to the monolithic case with a  
437 tip geometry  $R_f = 12$  mm. If we assume that the polymer deformation changes the  
438 effective frontal nose radius of the indenter ( $\hat{R}_f$ ) simply by following a geometrical  
439 relationship:

$$\hat{R}_f = \frac{R_i^2 + h_p^2}{2h_p} . \quad (3)$$

440 then, for this polymer thickness ( $h_p = 1.5$  mm),  $\hat{R}_f = 13.77$  mm will be obtained.  
441 Although a crude model, it appears to give a reasonable indication of the tip geometry  
442 at failure.

443 A similar comparison is performed for the bi-layers with  $h_p = 3$  and  $6$  mm in Figs. 11b  
444 and 11c respectively. Likewise, the response initially follows that of a monolithic plate

loaded by a blunt indenter. As indentation progresses, the slope of the indenter force-displacement curve, and the indenter displacement at failure, tends towards those of monolithic plates loaded by indenters with a tip geometry similar to  $\hat{R}_f$ .

These observations support the hypothesis that the deformation in the polymer layer alters the effective nose radius of the indenter, and hence indirectly increases the energy absorption in the metal backing layer. Specifically, it appears to increase the frontal nose radius. However, loading a monolithic plate with a non-deformable indenter with  $R_f \approx \hat{R}_f$  does not replicate all features of the bi-layer response, as the effective tip geometry appears to develop progressively during the indentation. For small indenter displacements, where little or no deformation occurs in the polymer, the response more closely matches that of a monolithic plate loaded by a blunt indenter. This progressive evolution of the effective tip geometry makes the application of analytical solutions developed for monolithic plates loaded by various fixed tip geometries (e.g. in [27]) unreliable.

## **5. Impact perforation**

We consider next the perforation resistance of polymer-metal bi-layer plates subject to impact loading by a blunt projectile. The objective is to assess whether the modes of deformation, failure and energy absorption observed under quasi-static loading are altered under dynamic loading.

### *5.1 Impact test methodology*

The target and clamping arrangements used in the impact experiments are identical to those described above for the quasi-static tests and illustrated in Fig. 1. Flat, square

specimen plates were clamped to a supporting plate by a circular clamping ring with internal diameter 100 mm. Blunt-nosed projectiles with diameter 12.5 mm (identical to the indenter geometry used in the quasi-static experiments) and mass  $20.2 \pm 0.2$  g were machined from mild steel. No plastic deformation of the projectile was observed during any of the impact experiments. The projectile was fired at velocities in the range 30-180  $\text{ms}^{-1}$  using a gas gun with barrel of internal diameter 12.7 mm. The specimen supporting plate was mounted to a steel frame and oriented normal to the barrel, so that the projectile impacted at  $90^\circ$  to the target. A high speed camera (Vision Research Phantom V710) oriented perpendicular to the flight of the projectile was used to record the motion of the projectile during its interaction with the target at a rate of 23000 frames per second. The projectile was designed with a tail of diameter 5 mm and length 20 mm, in which reference grooves were machined, so that the high speed camera could continue to track the projectile motion throughout its interaction with the target, even when the nose was obscured by the clamping frame. The high speed images therefore provided measurements of both the impact velocity  $V_i$  and the residual velocity  $V_r$ . We define a positive velocity in the direction of initial impact, so that a negative  $V_r$  indicates reflection of the projectile, and a positive  $V_r$  indicates perforation. Laser velocity gauges mounted at the barrel exit were used to verify the impact velocity obtained from the high speed photography, and showed good agreement.

A measure of the ballistic limit for each target was obtained by plotting residual velocity  $V_r$  against impact velocity  $V_i$  for a number of impact experiments. A curve was fitted through all data points with  $V_r \geq 0$ . The intersection of this curve with the zero residual velocity axis is considered to be the ballistic limit  $V_{bl}$  in this investigation. A polynomial form for the curve fit was used, based on the Lambert and Jonas relation [28]:

$$V_r = a(V_i^p - V_{bl}^p)^{1/p} . \quad (4)$$

where  $a$ ,  $p$  and  $V_{bl}$  are fitting parameters. To ensure adequate resolution of  $V_{bl}$ , repeat experiments were conducted at speeds near the ballistic limit in order to achieve at least 4 data points within  $\pm 4 \text{ ms}^{-1}$  of  $V_{bl}$ .

## 5.2 Impact response of monolithic and bi-layer plates

We first compare the impact response of one bi-layer configuration ( $h_m = 1 \text{ mm}$ ,  $h_p = 3 \text{ mm}$ ) with monolithic targets of the constituent materials. Here, the materials used are again aluminium alloy 6082-T6 and the polymer LDPE.

The initial and residual velocities of the projectile are shown in Fig. 12 for a monolithic metal plate with  $h_m = 1 \text{ mm}$  and a monolithic polymer plate with  $h_p = 3 \text{ mm}$ . These materials are identical to the individual layers in the bi-layer target. Results are also shown for a monolithic metal plate with thickness  $h_m = 2 \text{ mm}$ ; this target plate has approximately the same mass per unit area as the bi-layer target. The polynomial curves fitted to the residual velocity data, following Eq. (4), are shown. For the aluminium alloy plate with  $h_m = 1 \text{ mm}$ , the curve fit gives a ballistic limit  $V_{bl} = 57 \text{ ms}^{-1}$  (the other fitting parameters are  $p = 2.22$  and  $a = 0.98$ ). The thicker aluminium plate ( $h_m = 2 \text{ mm}$ ) results in  $V_{bl} = 96 \text{ ms}^{-1}$  ( $p = 2.22$ ,  $a = 0.97$ ). For the LDPE plate  $V_{bl} = 46 \text{ ms}^{-1}$  ( $p = 1.8$ ,  $a = 0.98$ ). Both materials failed by plugging, identical to the quasi-static case.

The bi-layer impact results are also plotted in Fig. 12. Two cases are shown: polymer on the impacted face, and polymer on the distal face. The impact results are consistent with the findings of the quasi-static experiments, with the energy required to perforate significantly higher when the polymer is placed on the impacted face rather than the distal face. The ballistic limits are  $94.5 \text{ ms}^{-1}$  and  $65.5 \text{ ms}^{-1}$  for these cases, respectively.

Placing the polymer on the distal face increases the ballistic limit only slightly compared to the monolithic metal with  $h_m = 1$  mm. However, when the polymer is on the impacted face, the ballistic limit is close to, but slightly less than, that of the equivalent mass monolithic aluminium alloy target ( $h_m = 2$  mm).

As in the quasi-static case, this performance difference between the bi-layer cases is due to the mode of deformation and failure of the metal layer. With the polymer on the distal face, the metal layer fails by plugging, similar to perforation of the monolithic metal plate. It is observed that in the bi-layer case the metal layer fails at  $V_i = 58 \text{ ms}^{-1}$  (which is slightly higher than the ballistic limit of the bare metal,  $V_{bl} = 57 \text{ ms}^{-1}$ ), with the polymer layer remaining intact at this impact velocity. However when the polymer is placed on the impacted face, plugging is suppressed and the metal layer undergoes increased dishing deformation, providing additional energy absorption.

### *5.3 Failure mode transition: comparison of quasi-static and dynamic loading*

The function of the polymer in altering the mode of deformation and failure of the bi-layer therefore appears to be similar for impact loading and quasi-static perforation. We next compare the influence of increasing the polymer thickness for these two load cases. The comparison is made for the bi-layer configuration with a fixed metal layer thickness  $h_m = 1$  mm and polymer layer thicknesses  $h_p = 1.6, 3.0, 4.5$  and  $5.9$  mm. The metal is aluminium alloy 6082-T6, and the polymer is LDPE, located on the impacted face. The perforation energy ( $W$ ) for quasi-static and impact loading cases are compared in Fig. 13a for increasing  $h_p$ . The perforation energy in the impact case is taken to be the initial kinetic energy of the projectile at the ballistic limit. A similar trend is seen for the two load cases, with  $W$  increasing with  $h_p$ , but at a reducing rate. The perforation energy  $W$  is also larger in the impact case for all polymer thicknesses  $h_p$ . Inertia and

strain rate sensitivity in both layers contribute to this dynamic elevation of the perforation energy. Photographs of the distal (metal) face of the bi-layer specimens at the onset of failure are shown in Fig. 13a for the impact case. The transition from plugging failure (small  $h_p$ ) to increased dishing and tensile failure (large  $h_p$ ) with increasing polymer thickness mirrors the quasi-static case (Fig. 6).

#### *5.4 Comparison with monolithic targets on an equal mass basis*

To assess the mass-efficiency of the bi-layer solution under impact, we next compare the bi-layer results described in Section 5.3 with monolithic specimens of the same metal and polymer type over the same range of plate mass. The plate thicknesses tested were  $h_m = 1.0, 1.6, 2.0$  and  $3.0$  mm for the monolithic aluminium alloy targets, and  $h_p = 3.0, 4.5, 5.9$  and  $9.1$  mm for the monolithic LDPE. The perforation energy  $W$  is plotted in Fig. 13b against the mass per unit area of the target for the bi-layer and monolithic plates. Note that the bi-layer experimental results begin at an areal density that represents zero polymer thickness. The results for both monolithic metal and polymer targets show an approximately linear trend in  $W$  with increasing plate mass, the aluminium alloy outperforming the polymer. In all cases, failure was by plugging. For the bi-layer target with small polymer thicknesses, the activation of dishing deformation results in a perforation energy that exceeds that of the equivalent mass monolithic metal. However, as  $h_p/h_m$  is increased further, the energy absorption tends towards the monolithic polymer result, and therefore begins to underperform monolithic metal. The optimum performance of the bi-layer relative to the equivalent mass monolithic metal target occurs when  $h_p = 1.6$  mm, corresponding to a target mass  $4.2 \text{ kg m}^{-2}$  and  $h_p/h_m = 1.6$  (Fig. 13b). Note that this bi-layer configuration also corresponds to a maximum in perforation energy per unit mass (obtained using Eq. (2)).

This optimum polymer thickness is smaller than that observed under quasi-static loading (for which  $h_p = 3$  mm offered the best perforation resistance per unit mass of plate). It therefore appears that dynamic deformation of the polymer reduces the thickness necessary to achieve the critical effective projectile nose shape.

The results of bi-layers with 2 mm metal substrate is also included in Fig 13b. In this case, only bi-layer targets with polymer thicknesses  $h_p = 1.6$  and 3.0 mm were used. The maximum polymer thickness that could be perforated in this case was limited by the impact speeds obtainable with the gas gun apparatus. The influence of the substrate thickness on the bi-layer response appears to be the same under impact conditions as that observed under quasi-static loading (Fig. 7). A given polymer layer thickness results in a greater improvement in perforation energy for the bi-layer with  $h_m = 2$  mm compared to the  $h_m = 1$  mm case. As a result, the bi-layer with the thicker substrate outperforms the equivalent mass monolithic metal for both polymer thicknesses tested (Fig. 13b).

## **6. Influence of polymer properties**

The results presented so far were obtained for one polymer layer type: low density polyethylene (LDPE). We consider next the influence of the mechanical properties of the polymer layer on the quasi-static and impact perforation of bi-layer plates with the polymer layer facing the indenter. Specifically, the influence of yield strength, ductility and strain hardening are considered, while maintaining the density and glass transition temperature of the polymers approximately constant. This is achieved by comparing three types of polyethylene: low density (LDPE), high density (HDPE) and ultra high molecular weight (UHMWPE). All polyethylene specimens were obtained from

591 extruded sheet. The measured densities of the three polymers are approximately equal:  
592  $930 \text{ kg m}^{-3}$  (LDPE),  $960 \text{ kg m}^{-3}$  (HDPE) and  $940 \text{ kg m}^{-3}$  (UHMWPE).

593 The viscoelastic properties of the polymers were characterised using Dynamic  
594 Mechanical Analysis spanning a temperature range of  $-175^\circ\text{C}$  to  $120^\circ\text{C}$  (with  
595 specimens tested in a cantilever bending configuration at a frequency of  $1 \text{ Hz}$ ), the  
596 results of which are given in Fig. 14. At room temperature, the HDPE has the highest  
597 elastic modulus, and the LDPE the lowest (Fig. 14a). The peaks in loss modulus show  
598 three relaxation events, denoted  $\alpha$ ,  $\beta$  and  $\gamma$  (Fig. 14b). The glass transition (the  $\gamma$  peak)  
599 occurs at approximately  $-120^\circ\text{C}$  for all three polyethylenes. The  $\beta$  relaxation is  
600 associated with molecular chain motion in the amorphous phase, and the  $\alpha$  relaxation  
601 to chain motion in the crystalline phase. The slightly higher  $\alpha$  relaxation temperature  
602 and lower amplitude of the loss modulus peak in the  $\beta$  relaxation indicate that the HDPE  
603 and UHMWPE specimens have a higher crystallinity than the LDPE specimen [29,30].

604 The nominal tensile stress-strain curves for all three polymers are shown in Fig. 2b. The  
605 measurement technique used is identical to that described previously for the LDPE. The  
606 HDPE has a higher yield strength than the LDPE, and it also has the highest tensile  
607 ductility of the polymers tested. The higher yield strength of the HDPE compared to the  
608 LDPE is consistent with it having a higher degree of crystallinity. The UHMWPE has  
609 a slightly lower yield strength than the HDPE, but a higher rate of strain hardening. The  
610 additional strain hardening in UHMWPE can be attributed to physical entanglement of  
611 the polymer molecular chains [31]. Further characterisation results for these three types  
612 of extruded polyethylene sheet are reported by Mohagheghian et al. [32] for a variety  
613 of load cases and strain rates.

In the following, a single bi-layer target configuration is considered, with a layer of aluminium alloy 6082-T6 that has thickness  $h_m = 1$  mm, and a polymer layer (LDPE, HDPE or UHMWPE) that has thickness  $h_p = 3$  mm and is located on the impacted face.

### *6.1 Quasi-static loading*

The quasi-static perforation results for the monolithic aluminium alloy and bi-layer plates pressed by a blunt indenter are shown in Fig. 15a. All three polymer types lead to an increase in energy absorption for the bi-layer compared to the bare metallic substrate. This is due to the same process in each case: a switch from plugging to tensile failure, accompanied by a delay in failure of the metal layer and increased dishing deformation. This can be seen in Fig. 16a, which shows the permanent deformation of the metal layer in the bi-layer and monolithic specimens measured at the point of fracture of the metal using profilometry. All three polymers enable much larger plastic deformation in the metal up to the point of first fracture compared to the monolithic case. It is also notable in Fig. 16a that the plastic deformation of the metal layer is insensitive to the polymer choice.

The gradient of the force-deflection plot (Fig. 15a) is slightly larger in phase 1 for the HDPE and UHMWPE bi-layers compared to the LDPE case. This can be explained by the higher yield-strengths of these polymers offering higher resistance to local indentation. The indenter displacement at fracture of the metal layer is also slightly different for the three bi-layer cases, with UHMWPE achieving the largest value. However, the differences between the three bi-layer specimens are not large: the polymer choice has only a small influence on the total perforation energy, as shown in Fig. 15b. This further supports the argument that the polymer contributes little to the overall increase in energy absorption through dissipative mechanisms within the

polymer itself. Its primary function is to deform under the indenter in order to promote dishing and plastic dissipation in the metal, and all three polymers have sufficiently low strength and high ductility to perform this function during quasi-static loading.

## 6.2 Impact loading

Impact experiments were performed on the same monolithic and bi-layer target configurations in order to assess the sensitivity to the polymer type under dynamic loading conditions. The impact perforation energy for the bi-layer specimens is shown in Fig. 15b. Profilometry results of the deformed metal layers at an impact velocity for which perforation just occurs are shown in Fig. 16b. The dynamic loading results in larger plastic deformations at fracture and increased perforation energy for the monolithic and the bi-layer specimens. However, the performance advantage of the bi-layers relative to the bare metallic substrate, while maintained for the UHMWPE case, is diminished for both the LDPE and HDPE cases.

To understand this increased sensitivity to polymer type, the tensile tests reported in Section 2 were repeated on the three polymers at an increased strain rate. The results are summarised in Table 1. Consider first the dynamic elevation in the strength of the polymers. The yield strength increases in a similar manner for each polymer with increasing strain rate, with the rate of increase slightly greater for HDPE. Differences in the dynamic strength of the polymers therefore do not explain the relative performances of the bi-layer targets.

Fig. 16c shows the post-impact profilometry results for two bi-layers with either LDPE or UHMWPE facing the projectile. Both bi-layers were impacted at the same velocity of  $85 \text{ ms}^{-1}$ , which is below their ballistic limits. No sign of fracture in the metal layer was observed in either case at this impact velocity. The LDPE layer shows more local

shear deformation at the perimeter of the projectile compared to the UHMWPE. As a result, a plug of material, ahead of the projectile, has started to develop in the LDPE layer (Fig. 16c), which is not the case for UHMWPE at this impact speed (Fig. 16c). This affects the local deformation and curvature of the metal layer, which in turn can explain the lower perforation velocity for a bi-layer using LDPE.

Mohagheghian et al. [32] conducted shear punch experiments on LDPE, HDPE and UHMWPE at strain rates spanning five orders of magnitude. Their results show that the resistance to shear deformation (localisation followed by failure) is significantly higher for UHMWPE compared to LDPE and HDPE. The shear resistance of UHMWPE also significantly increases at higher strain rates due to the higher strain rate sensitivity of strain hardening for this material. In contrast, for LDPE and HDPE, when increasing the strain rate, softening in the shear response is observed which is believed to be caused by adiabatic heating. The same mechanism seems to be responsible here. For LDPE, strain localisation is accelerated by local adiabatic heating at high strain rates, as the flow stress of polyethylene is significantly reduced by increasing temperature during high strain rate deformation. A high degree of strain hardening, which is maintained at high strain rates, delays localisation, diffusing regions of high strain in UHMWPE. This explains the higher dynamic elevation in perforation energy for the bi-layer with UHMWPE (Fig. 15b).

### *6.3 Comparison with equal mass monolithic metal*

Finally, the influence of polymer type on the competitiveness of the bi-layer solution with monolithic aluminium alloy on an equal mass basis is considered. Fig. 15b compares the perforation energy of the bi-layer specimens with monolithic metal plates

with thickness  $h_m = 2$  mm, which have the same total mass. Quasi-statically, the bi-layer plates outperform the monolithic metal for all three polymer types. However, the choice of polymer becomes more important under impact loading. While the UHMWPE bi-layer maintains a similar performance advantage compared to the equal mass monolithic target, the HDPE and LDPE bi-layers see a reduction in relative performance. The lack of resistance to localisation of these polymers under impact conditions therefore makes them less attractive in comparison with a metallic target on an equal mass basis.

## 7. Discussion

In the previous sections, we argued that the primary function of the polymer in the bi-layer system is to alter the effective tip geometry of the projectile (or indenter). In this section, we discuss alternative mechanisms that have been proposed in the literature in order to explain the performance of polymer-metal bi-layer systems loaded dynamically.

Two main mechanisms have been proposed: (i) an impact induced glass transition in the polymer layer [2,20,33] and (ii) stabilisation of the onset of tensile necking in the metal layer [34,35]. However, neither of these mechanisms can adequately explain the bi-layer performance in the current investigation, for the following reasons:

1. *Impact induced glass transition:* In the current study, we carried out both quasi-static and dynamic perforation experiments, and observed similar performance enhancements for bi-layer systems in both cases. The strain rate induced in the polymer layer is therefore deduced to be of secondary importance to the mechanism responsible. Furthermore, the polymers studied here have a very low glass transition temperature ( $T_g$  around  $-120^\circ\text{C}$ , as shown in Fig. 14), and

so it is unlikely that the transition from a rubbery to glassy state occurs, even under impact loading.

2. *Neck retardation*: For a polymer layer to retard the onset of necking in the metal layer, a bonded interface is required between the layers [34]. However, in this investigation, the layers are only in frictional contact. The second requirement for neck retardation is a polymer with sufficiently large incremental stiffness. For the polyethylenes used in this investigation, yielding occurs at a true strain of around 0.05, and the incremental stiffness subsequently drops significantly and remains low up to a true strain of about 1 [31,36]. This is the range of strains for which necking occurs in the aluminium layer. Based on the analysis of Xue and Hutchinson [34] for a bi-layer plate under bi-axial stretching, the polymer tangent modulus required to activate the neck retardation mechanism is calculated to be around 170 MPa for the material combination used in this study. It should be noted that, as the loading and boundary conditions differ from those of the Xue and Hutchinson [34] analysis, this value can only be treated as indicative of the critical tangent modulus for the current test configuration. Nonetheless, the incremental stiffness of the polymer is significantly lower than this value, and so the neck retardation mechanism is unlikely to be active in the current experiments.

Consequently, we conclude that the effective nose shape change is the primary synergistic mechanism for the bi-layer targets considered here. The same mechanism has been observed for thin metallic plates when impacted by deformable projectiles. Liu and Stronge [37] investigated the failure modes and ballistic limit of thin metallic targets using projectiles with different strengths. They observed that by decreasing the strength of the projectile more deformation (normally called ‘mushrooming’) occurred

in the projectile. As a result, both the diameter and nose radius of the projectile are changed. This has a direct effect on the failure mode in the metal. For a blunt projectile with higher strength, shear failure is most likely to occur. Conversely, for more deformable projectiles, tensile tearing is more favourable. The increase in the ballistic limit for softer projectiles is considered to be the result of more dishing in the plate. Positioning a soft and deformable polymer layer between a non-deformable blunt projectile and the metal layer is believed to have a very similar effect.

## **8. Conclusions**

An experimental investigation has been conducted into the influence of a polymer layer on the quasi-static and impact perforation of thin metallic plates by a blunt indenter. The following conclusions are made:

- For both quasi-static and impact loading, the mode of deformation and failure of a bi-layer specimen are sensitive to the order of the layers. If the metallic layer faces the indenter, both layers fail by plugging (as observed for monolithic plates of the same materials). In this case, the perforation energy of the bi-layer is significantly below that of a monolithic metal plate of the same mass. However, if the polymer is located on the impacted face of the plate, more dishing occurs in the metallic layer, followed by tensile failure. This increases the energy dissipated in the metal layer, and results in a significant rise in the perforation energy.
- When a bi-layer plate has the polymer facing the indenter, the polymer forms a cap under the indenter tip, altering its effective nose shape. This is responsible for the change in the mode of deformation of the metal layer. The shape of this polymer cap (which is retrieved after each experiment for inspection) depends on the

thickness of the polymer layer. As the polymer thickness is increased, the metal layer undergoes a transition from plugging (thin polymer layer) to dishing and tensile failure (thick polymer layer).

- There is an optimum ratio of polymer to metal thickness to maximise the perforation resistance of this bi-layer configuration relative to a monolithic metal plate of the same mass. At the optimum, the polymer layer alters the indenter tip geometry such that the amount of dishing deformation in the metal layer is a maximum. (A similar behaviour is observed by loading the metallic plate directly with indenters having a range of tip radii, from blunt to hemi-spherical, with peak perforation resistance seen at an intermediate tip radius). The optimised bi-layer plate has a higher perforation energy than an equivalent mass monolithic plate.
- Under impact loading the response of the bi-layer with the polymer facing the indenter is sensitive to the polymer type. A high degree of strain hardening (as displayed by UHMWPE) appears to be a key polymer characteristic for increasing the perforation energy, rather than the yield strength of the polymer. Strain hardening resists strain localisation in the polymer as it deforms plastically under the indenter, delaying polymer plug formation and in turn delaying fracture of the metal substrate.

## **Acknowledgments**

The authors are grateful for joint financial support from the Engineering and Physical Sciences Research Council (EPSRC) and the Defence Science and Technology Laboratory (DSTL) through project EP/G042756/1 (Polymer Nanocomposites for

Light Armour Applications). We acknowledge the EPSRC instrument loan pool for the use of the high speed camera (Vision Research Phantom V710).

## References

- [1] W.J. Mock, W. Holt, G. Sutherland, G. Lee, E. Balizer, J. Fedderly, Penetration protection experiments using polymer materials, 2005.
- [2] C.M. Roland, D. Fragiadakis, R.M. Gamache, Elastomer–steel laminate armor, *Compos. Struct.* 92 (2010) 1059–1064. doi:10.1016/j.compstruct.2009.09.057.
- [3] G.G. Corbett, S.R. Reid, W. Johnson, Impact loading of plates and shells by free-flying projectiles: A review, *Int. J. Impact Eng.* 18 (1996) 141–230. doi:10.1016/0734-743X(95)00023-4.
- [4] J. Radin, W. Goldsmith, Normal projectile penetration and perforation of layered targets, *Int. J. Impact Eng.* 7 (1988) 229–259. doi:10.1016/0734-743X(88)90028-0.
- [5] A.A. Almohandes, M.S. Abdel-Kader, A.M. Eleiche, Experimental investigation of the ballistic resistance of steel-fiberglass reinforced polyester laminated plates, *Compos. Part B Eng.* 27 (1996) 447–458. doi:10.1016/1359-8368(96)00011-X.
- [6] P. Elek, S. Jaramaz, D. Micković, Modeling of perforation of plates and multi-layered metallic targets, *Int. J. Solids Struct.* 42 (2005) 1209–1224. doi:10.1016/j.ijsolstr.2004.06.053.
- [7] I. Marom, S.R. Bodner, Projectile perforation of multi-layered beams, *Int. J. Mech. Sci.* 21 (1979) 489–504. doi:10.1016/0020-7403(79)90011-0.
- [8] S. Dey, T. Børvik, X. Teng, T. Wierzbicki, O.S. Hopperstad, On the ballistic

809 resistance of double-layered steel plates: An experimental and numerical  
810 investigation, *Int. J. Solids Struct.* 44 (2007) 6701–6723.  
811 doi:10.1016/j.ijsolstr.2007.03.005.

812 [9] X. Teng, S. Dey, T. Børvik, T. Wierzbicki, Protection performance of double-  
813 layered metal shields against projectile impact, *J. Mech. Mater. Struct.* 2 (2007)  
814 1309–1329. doi:10.2140/jomms.2007.2.1309.

815 [10] N.K. Gupta, M.A. Iqbal, G.S. Sekhon, Effect of projectile nose shape, impact  
816 velocity and target thickness on the deformation behavior of layered plates, *Int.*  
817 *J. Impact Eng.* 35 (2008) 37–60. doi:10.1016/j.ijimpeng.2006.11.004.

818 [11] R.S.J. Corran, C. Ruiz, P.J. Shadbolt, On the design of containment shields,  
819 *Comput. Struct.* 16 (1983) 563–572. doi:10.1016/0045-7949(83)90196-7.

820 [12] C.-C. Liang, M.-F. Yang, P.-W. Wu, T.-L. Teng, Resistant performance of  
821 perforation of multi-layered targets using an estimation procedure with marine  
822 application, *Ocean Eng.* 32 (2005) 441–468.  
823 doi:10.1016/j.oceaneng.2004.05.009.

824 [13] N.K. Gupta, V. Madhu, An experimental study of normal and oblique impact of  
825 hard-core projectile on single and layered plates, *Int. J. Impact Eng.* 19 (1997)  
826 395–414. doi:10.1016/S0734-743X(97)00001-8.

827 [14] J.A. Zukas, D.R. Scheffler, Impact effects in multilayered plates, *Int. J. Solids*  
828 *Struct.* 38 (2001) 3321–3328. doi:10.1016/S0020-7683(00)00260-2.

829 [15] X. Teng, T. Wierzbicki, M. Huang, Ballistic resistance of double-layered armor  
830 plates, *Int. J. Impact Eng.* 35 (2008) 870–884.  
831 doi:10.1016/j.ijimpeng.2008.01.008.

832 [16] E.A. Flores-Johnson, M. Saleh, L. Edwards, Ballistic performance of multi-

- 833 layered metallic plates impacted by a 7.62-mm APM2 projectile, *Int. J. Impact*  
834 *Eng.* 38 (2011) 1022–1032. doi:10.1016/j.ijimpeng.2011.08.005.
- 835 [17] G. Ben-Dor, a. Dubinsky, T. Elperin, On the order of plates providing the  
836 maximum ballistic limit velocity of a layered armor, *Int. J. Impact Eng.* 22 (1999)  
837 741–755. doi:10.1016/S0734-743X(99)00024-X.
- 838 [18] G. Ben-Dor, A. Dubinsky, T. Elperin, Effect of the order of plates on the ballistic  
839 resistance of ductile layered shields perforated by nonconical impactors, *J. Mech.*  
840 *Mater. Struct.* 1 (2006) 1161–1177. doi:10.2140/jomms.2006.1.279.
- 841 [19] Y. Liu, B. Liaw, Drop-weight impact tests and finite element modeling of cast  
842 acrylic/aluminum plates, *Polym. Test.* 28 (2009) 808–823.  
843 doi:10.1016/j.polymertesting.2009.07.003.
- 844 [20] C.M. Roland, D. Fragiadakis, R.M. Gamache, R. Casalini, Factors influencing  
845 the ballistic impact resistance of elastomer-coated metal substrates, *Philos. Mag.*  
846 93 (2013) 468–477. doi:10.1080/14786435.2012.722235.
- 847 [21] L. Xue, W.J. Mock, T. Belytschko, Penetration of DH-36 steel plates with and  
848 without polyurea coating, *Mech. Mater.* 42 (2010) 981–1003.  
849 doi:10.1016/j.mechmat.2010.08.004.
- 850 [22] E. Onat, R. Haythornthwaite, The Load Carrying Capacity of Circular Plates at  
851 Large Deflection., *J. Appl. Mech.* 23 (1954) 49–55.  
852 <http://www.stormingmedia.us/70/7001/A700159.pdf> (accessed August 20,  
853 2012).
- 854 [23] G.G. Corbett, S.R. Reid, Quasi-static and dynamic local loading of monolithic  
855 simply-supported steel plate, *Int. J. Impact Eng.* 13 (1993) 423–441.  
856 doi:10.1016/0734-743X(93)90116-O.

- 857 [24] M. Langseth, P.K. Larsen, The behaviour of square steel plates subjected to a  
858 circular blunt ended load, *Int. J. Impact Eng.* 12 (1992) 617–638.  
859 doi:10.1016/0734-743X(92)90271-T.
- 860 [25] B.C. Simonsen, L.P. Lauridsen, Energy absorption and ductile failure in metal  
861 sheets under lateral indentation by a sphere, *Int. J. Impact Eng.* 24 (2000) 1017–  
862 1039. doi:10.1016/S0734-743X(00)00024-5.
- 863 [26] R.S.J. Corran, P.J. Shadbolt, C. Ruiz, Impact loading of plates — An  
864 experimental investigation, *Int. J. Impact Eng.* 1 (1983) 3–22. doi:10.1016/0734-  
865 743X(83)90010-6.
- 866 [27] I. Mohagheghian, W.J. Stronge, G.J. McShane, Predicting indenter nose shape  
867 sensitivity for quasi-static perforation of thin metallic plates,. *Eur. J. Mech A-  
868 Solid* 61 (2017) 134-150. doi: [10.1016/j.euromechsol.2016.09.004](https://doi.org/10.1016/j.euromechsol.2016.09.004)
- 869 [28] J.P. Lambert, G.H. Jonas, Towards standardization in terminal ballistics testing:  
870 velocity representation, 1976.  
871 <http://oai.dtic.mil/oai/oai?verb=getRecord&metadataPrefix=html&identifier=ADA021389>  
872 (accessed July 11, 2013).
- 873 [29] K. -h. Nitta, A. Tanaka, Dynamic mechanical properties of metallocene  
874 catalyzed linear polyethylenes, *Polymer (Guildf)*. 42 (2001) 1219–1226.  
875 doi:10.1016/S0032-3861(00)00418-3.
- 876 [30] M. Munaro, L. Akcelrud, Correlations between composition and crystallinity of  
877 LDPE/HDPE blends, *J. Polym. Res.* 15 (2008) 83–88. doi:10.1007/s10965-007-  
878 9146-2.
- 879 [31] Z. Bartczak, Effect of Chain Entanglements on Plastic Deformation Behavior of  
880 Ultra-High Molecular Weight Polyethylene, *J. Polym. Sci. Part B Polym. Phys.*

- 881 48 (2010) 276–285. doi:10.1002/polb.21873.
- 882 [32] I. Mohagheghian, G.J. McShane, W.J. Stronge, Impact perforation of monolithic  
883 polyethylene plates: Projectile nose shape dependence, *Int. J. Impact Eng.* 80  
884 (2015) 162–176. doi:10.1016/j.ijimpeng.2015.02.002.
- 885 [33] M. Grujicic, B. Pandurangan, T. He, B.A. Cheeseman, C.-F. Yen, C.L. Radow,  
886 Computational investigation of impact energy absorption capability of polyurea  
887 coatings via deformation-induced glass transition, *Mater. Sci. Eng. A.* 527  
888 (2010) 7741–7751. doi:10.1016/j.msea.2010.08.042.
- 889 [34] Z. Xue, J.W. Hutchinson, Neck retardation and enhanced energy absorption in  
890 metal–elastomer bilayers, *Mech. Mater.* 39 (2007) 473–487.  
891 doi:10.1016/j.mechmat.2006.08.002.
- 892 [35] Z. Xue, J.W. Hutchinson, Neck development in metal/elastomer bilayers under  
893 dynamic stretchings, *Int. J. Solids Struct.* 45 (2008) 3769–3778.  
894 doi:10.1016/j.ijsolstr.2007.10.006.
- 895 [36] Z. Bartczak, Effect of Chain Entanglements on Plastic Deformation Behavior of  
896 Linear Polyethylene, *Macromolecules.* 38 (2005) 7702–7713.  
897 doi:10.1021/ma050815y.
- 898 [37] D. Liu, W.J. Stronge, Ballistic limit of metal plates struck by blunt deformable  
899 missiles: experiments, *Int. J. Solids Struct.* 37 (2000) 1403–1423.  
900 doi:10.1016/S0020-7683(98)00322-9.

901

## Figure Captions

Figure 1: Schematic of the specimen plate clamping and loading arrangement.

Figure 2: Quasi-static uniaxial tensile response of (a) Al alloy 6082-T6 (b) polyethylenes LDPE, HDPE and UHMWPE.

Figure 3: Quasi-static indentation responses. (a) Monolithic Al alloy 6082-T6 ( $h_m = 1$  mm), including a linear fit to phase 1b. (b) Comparison between monolithic 6082-T6 ( $h_m = 1$  mm), monolithic LDPE ( $h_p = 3$  mm), and bi-layer plates of the same materials ( $h_m = 1$  mm,  $h_p = 3$  mm) with the polymer on the contact surface (in front of the metal) and the distal surface (behind the metal).

Figure 4: Failure modes observed during quasi-static indentation. Monolithic plates of (a) Al alloy 6082-T6 ( $h_m = 1$  mm) and (b) LDPE ( $h_p = 3$  mm). Bi-layer plates of the same materials ( $h_m = 1$  mm,  $h_p = 3$  mm) with (c) the metal on the contacted face, (d) LDPE on the contacted face, shown at the onset of failure of the metal layer and (e) shown fully perforated. Image (c) shows the contacted face, while (d) and (e) show the distal face.

Figure 5: The effect of polymer layer thickness ( $h_p$ ) on the quasi-static indentation response of polymer-metal bi-layer: (a) Force ( $F$ ) against indenter displacement ( $u_i$ ), (b) Energy absorbed ( $W$ ) during phases 1 and 2 of indentation, and the total for the complete perforation of the plate.  $\bar{W}$  is the total perforation energy normalised by the mass per unit area of the plate, (c) Comparison of the indenter displacement ( $u_{if}$ ) and distal face displacement in the centre of the plate ( $u_{Bf}$ ) under load at the point of fracture

of the metal layer. In all cases the polymer is located on the contacted face and the metal layer is Al alloy 6082-T6 ( $h_m = 1$  mm).

Figure 6: Failure modes observed during quasi-static indentation for monolithic Al alloy plates (6082-T6) and bi-layer plates with  $h_m = 1, 2$  mm (6082-T6 on the distal face, LDPE on the contact face) at the onset of fracture of the metal layer. The distal face is shown in each case. Also shown is the polymer cap which formed at the tip of the indenter in each bi-layer case.

Figure 7: (a) Comparison of the energy absorption ( $W$ ) in phase 1 of quasi-static indentation for specimens with two metal layer thicknesses ( $h_m = 1$  mm and 2 mm, both 6082-T6) and different thicknesses of polymer  $h_p$  (LDPE).

Figure 8: Axi-symmetric indenter tip geometries with (a) different chamfer radii ( $R_c$ ) and (b) different tip radii ( $R_f$ ).

Figure 9: (a),(b) Quasi-static indentation responses ( $u_i$  is the indenter displacement and  $F$  the force) and (c) energy absorbed ( $W$ ) in phase 1 for monolithic Al alloy 6082-T6 ( $h_m = 1$  mm) plates perforated by indenters with different corner radii  $R_c$  and tip radii  $R_f$ .

Figure 10: Failure modes observed during quasi-static indentation of monolithic Al alloy 6082-T6 ( $h_m = 1$  mm) for indenters with different values of  $R_i/R_f$  and  $R_c/R_i$ . The distal face at the onset of fracture is shown in each case.

Figure 11: Comparison of indentation response, using a blunt indenter, of the bi-layers with (a)  $h_p = 1.5$  mm, (b)  $h_p = 3$  mm and (c)  $h_p = 6$  mm with monolithic metal using indenters with different  $R_f$ . In all bi-layer cases the metal layer (Al alloy 6082-T6  $h_m = 1$  mm) is located on the distal face.

Figure 12: Residual velocity ( $V_r$ ) versus impact velocity ( $V_i$ ) of the projectile for: monolithic Al alloy 6082-T6 ( $h_m = 1$  mm and 2 mm), monolithic LDPE ( $h_p = 3$  mm) and bi-layer plates of the same materials ( $h_m = 1$  mm,  $h_p = 3$  mm) with the polymer on the impacted surface (marked 'polymer-metal') or the distal surface (marked 'metal-polymer'). The zero energy absorption line ( $V_r = V_i$ ) is shown for reference.

Figure 13: (a) Comparison of the perforation energy ( $W$ ) between quasi-static and impact loading for plates with metal thickness  $h_m = 1$  mm (6082-T6) and different thicknesses of polymer  $h_p$  (LDPE) on the impacted face. (b) Variation of the perforation energy with total plate mass per unit area for monolithic 6082-T6, monolithic LDPE and two configurations of bi-layer: (i)  $h_m = 1$  mm with increasing  $h_p$  and (ii)  $h_m = 2$  mm with increasing  $h_p$ .

Figure 14: Dynamic mechanical analysis: temperature scan at a frequency of 1 Hz for LDPE, HDPE and UHMWPE showing (a) storage and (b) loss modulus.

Figure 15: (a) Quasi-static indentation responses of monolithic Al alloy 6082-T6 ( $h_m = 1$  mm) and bi-layer plates with  $h_m = 1$  mm (6082-T6) and  $h_p = 3$  mm (three polymer types). In all cases the polymer is located on the contacted face. (b) A comparison of the quasi-static and impact perforation energy of the bi-layer plates. Shown as dashed

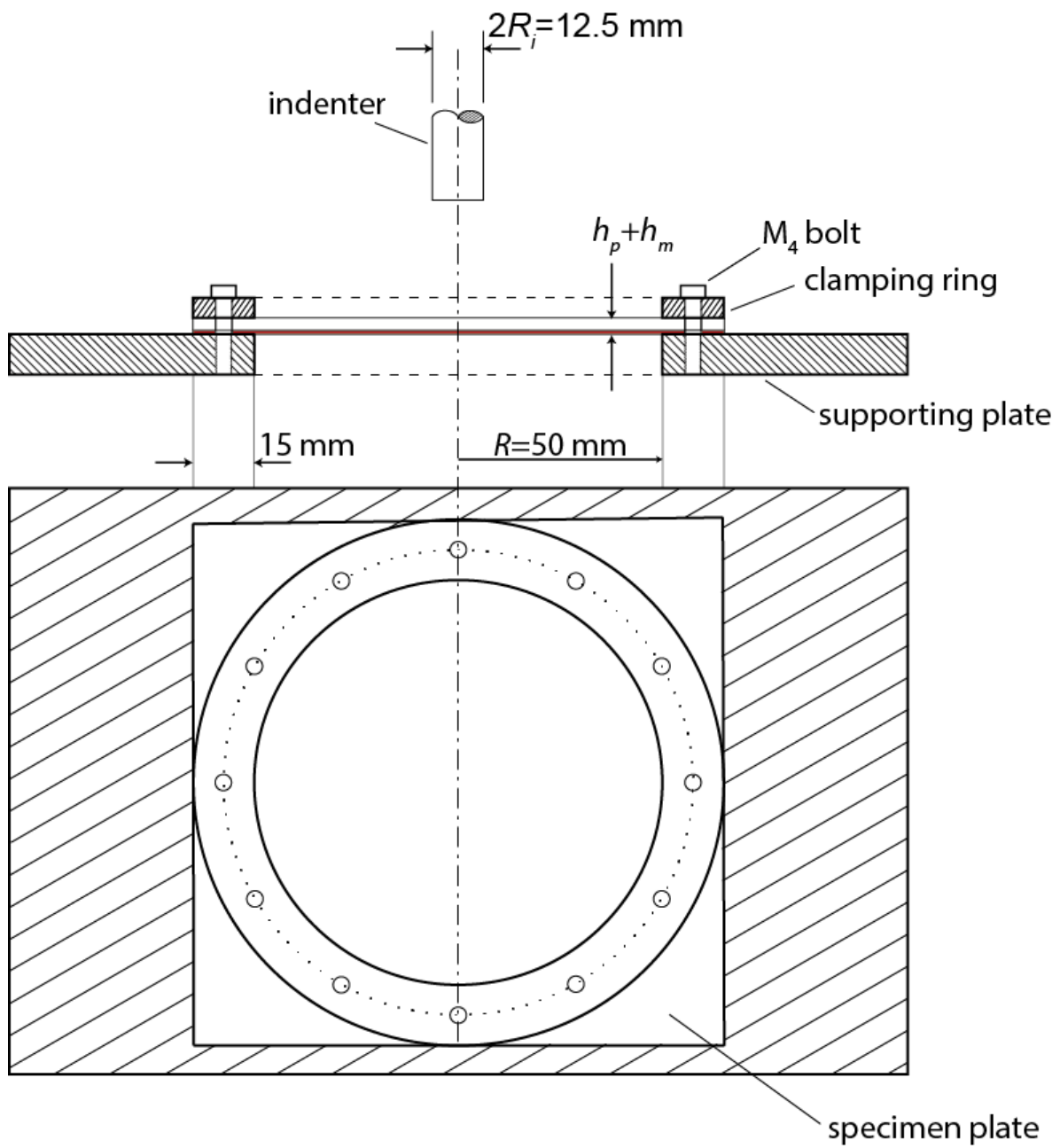
lines are the quasi-static and impact perforation energies for monolithic metal plates with  $h_m = 2$  mm (the same mass as the bi-layers).

Figure 16: Permanent distal face deflection ( $d_p$ ) of the metal layer at the onset of fracture of the metal for monolithic metal and bi-layer plates, measured along the plate diameter using profilometry. Horizontal distance  $x$  is measured relative to the centre of the plate. (a) Quasi-static and (b) impact loading. The monolithic plate is 6082-T6 ( $h_m = 1$  mm), and the bi-layer plates have  $h_m = 1$  mm (6082-T6) and  $h_p = 3$  mm (LDPE, contacted face). (c) Compares the permanent deflection of the metal layer (distal face) and the polymer layer (distal and impacted faces) for two bi-layers with either LDPE or UHMWPE on the impacted face, for a projectile velocity of  $85 \text{ ms}^{-1}$ .

Table 1: Strain rate dependence of the polymer mechanical properties.

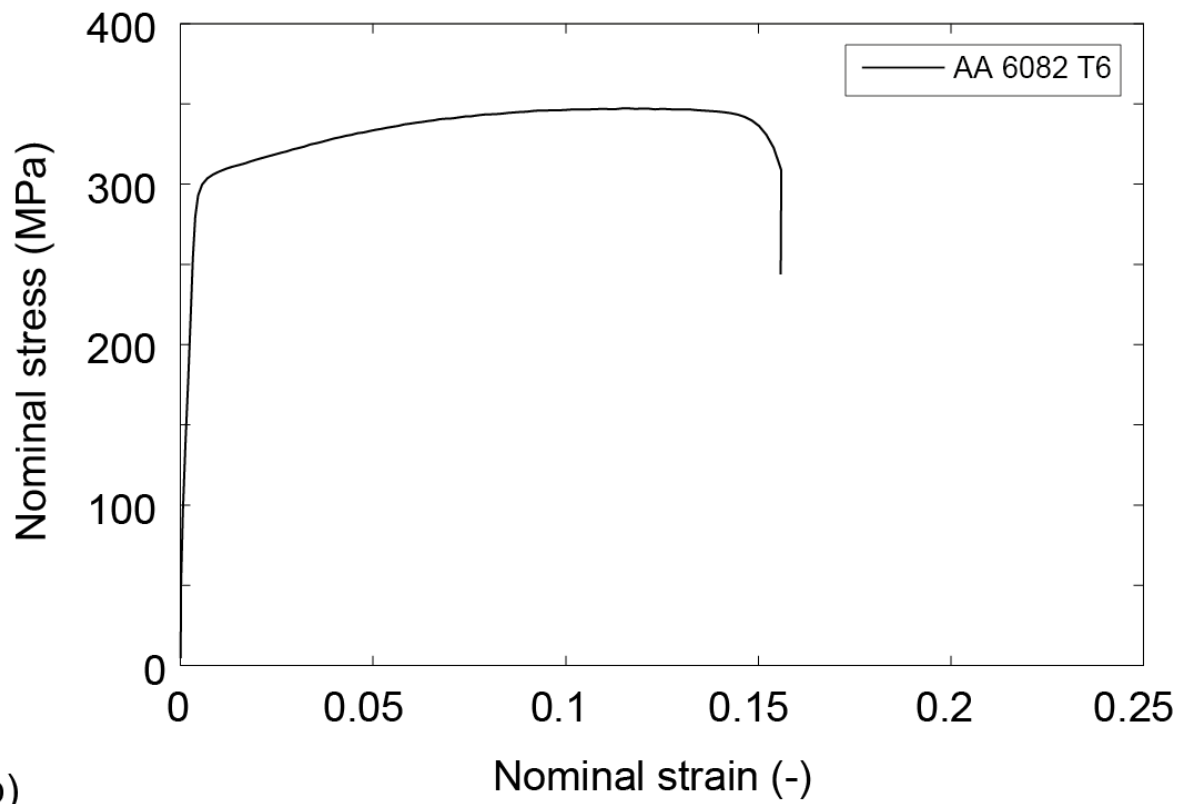
.

**Figure 1:**

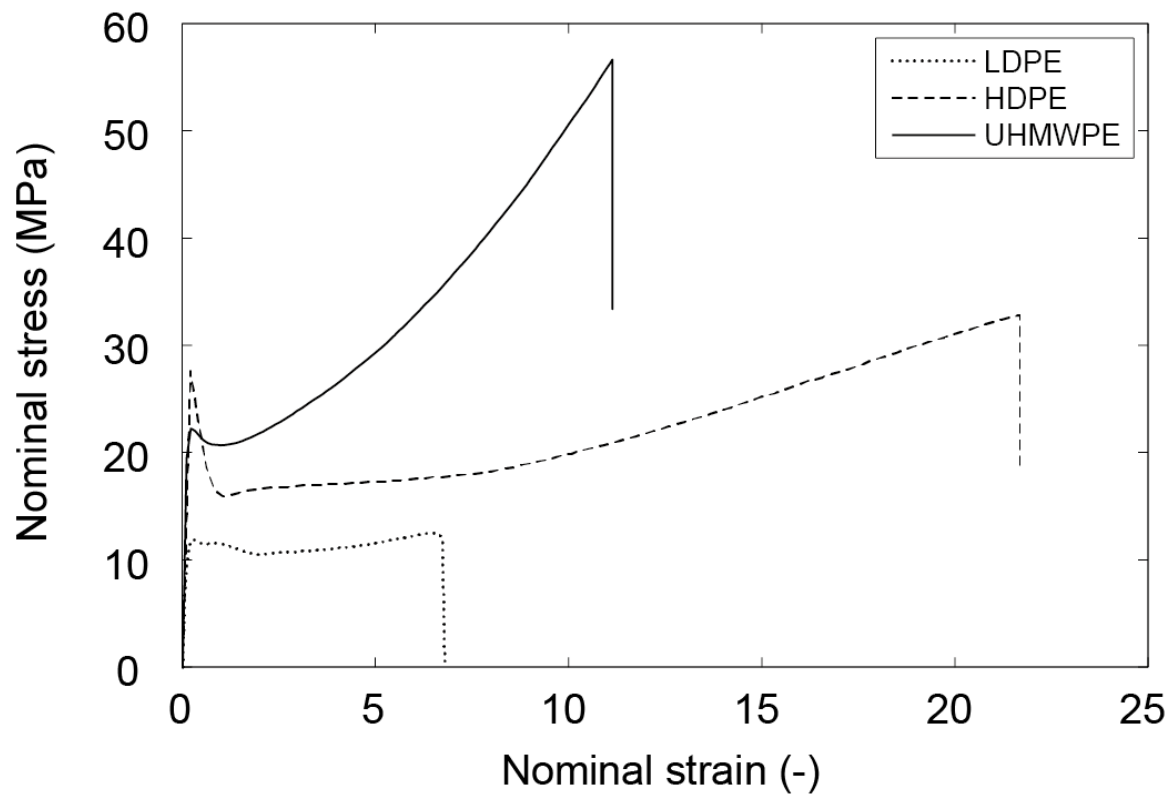


**Figure 2:**

(a)

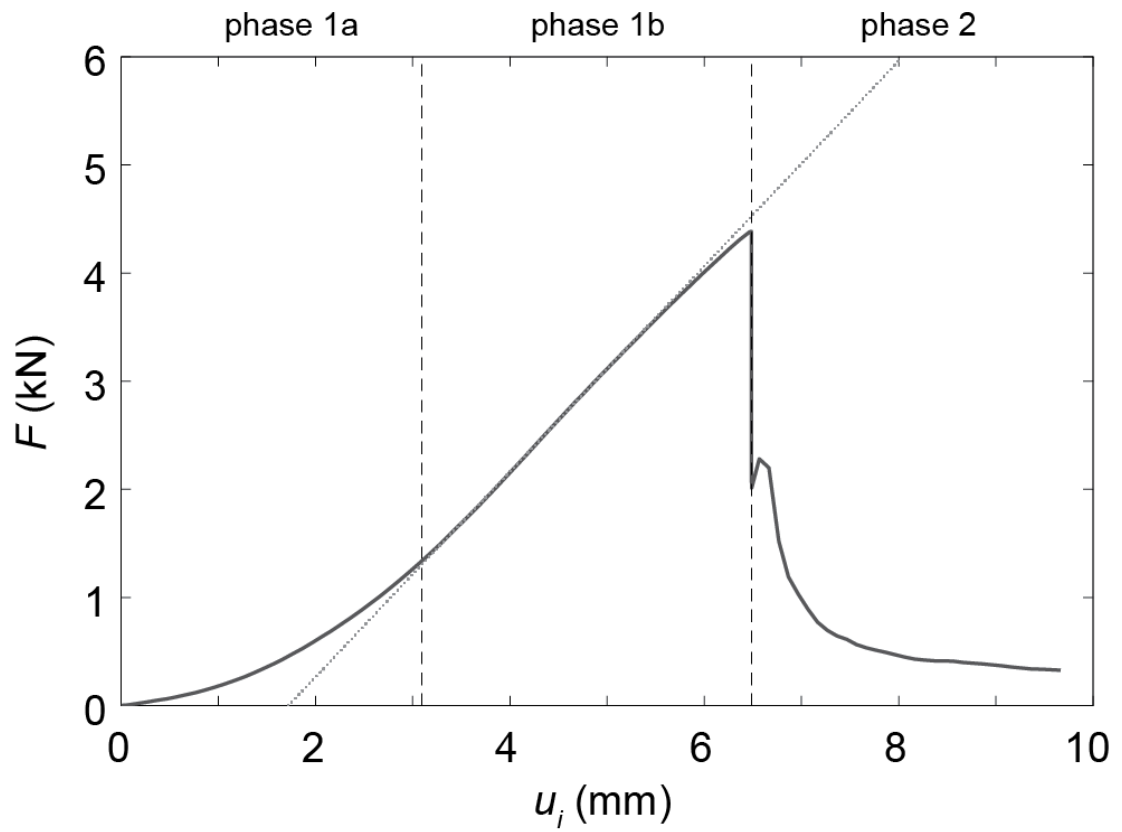


(b)

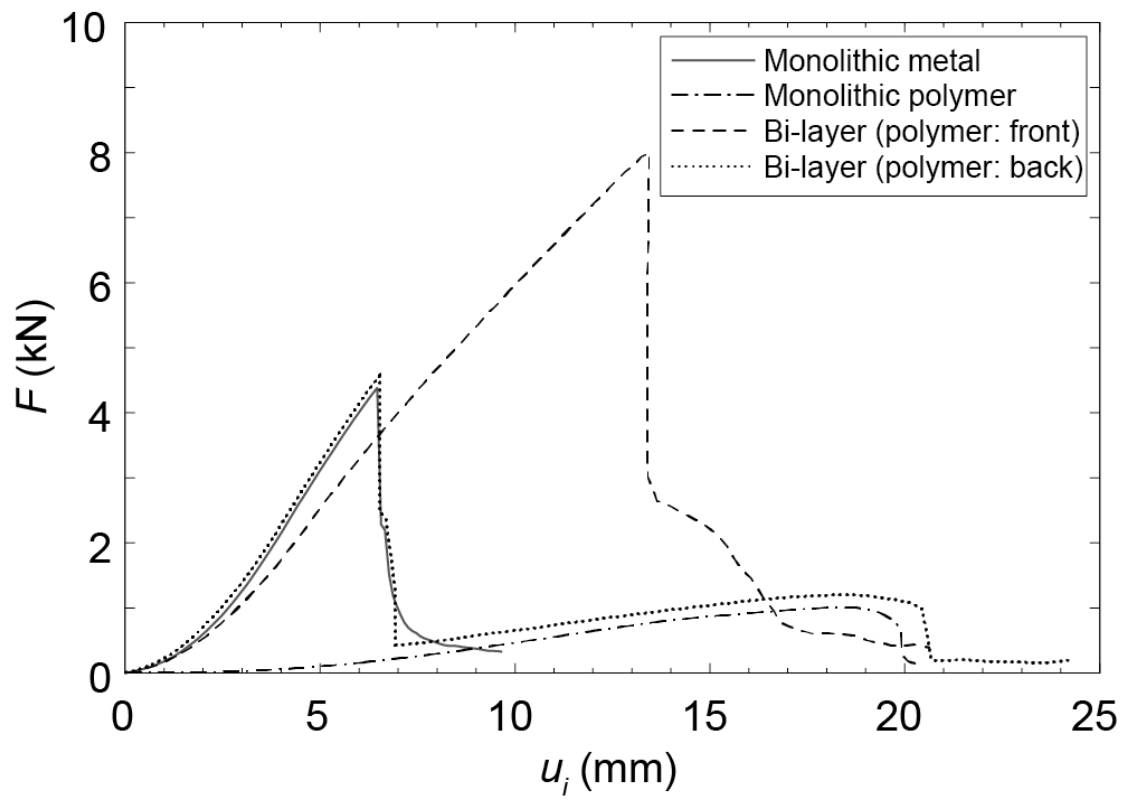


**Figure 3:**

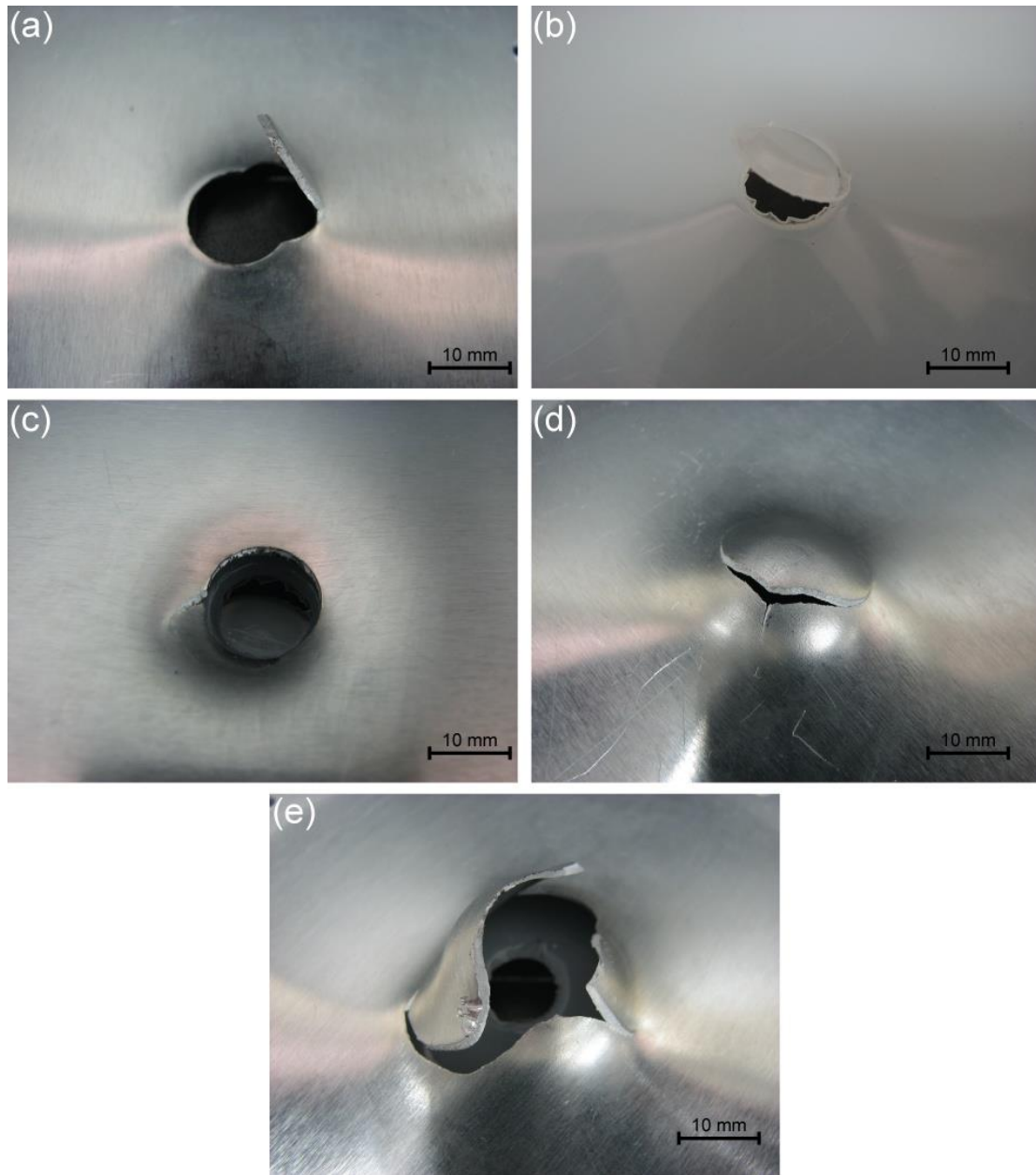
(a)



(b)

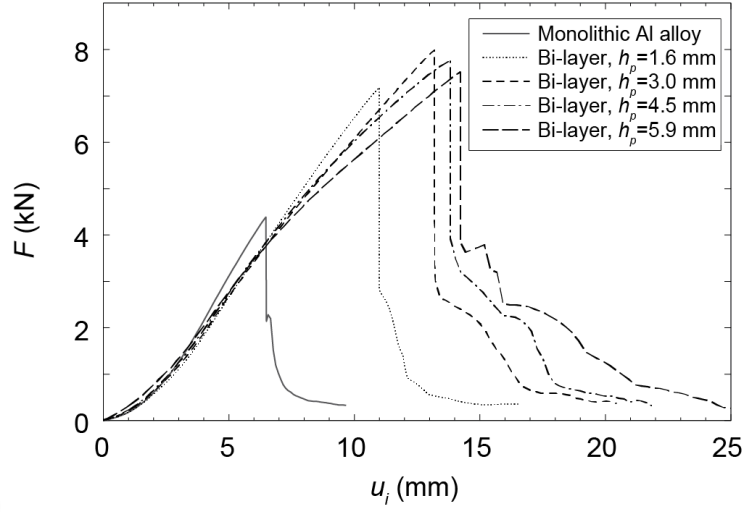


**Figure 4:**

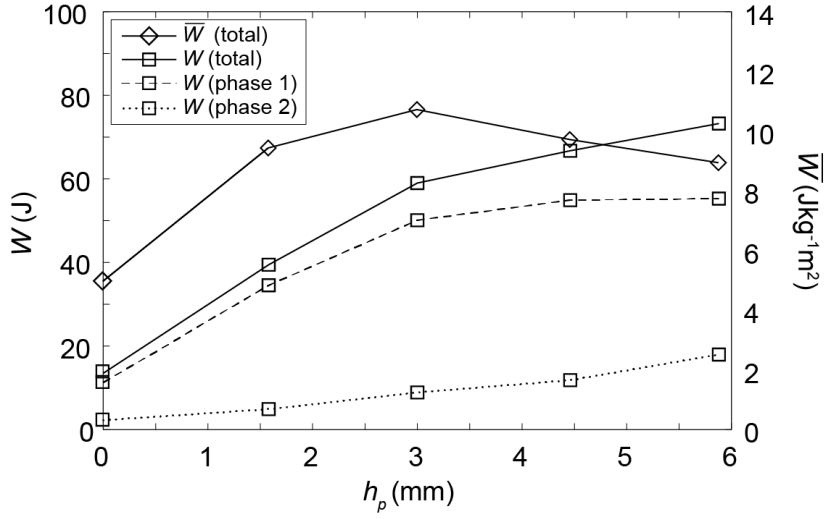


**Figure 5:**

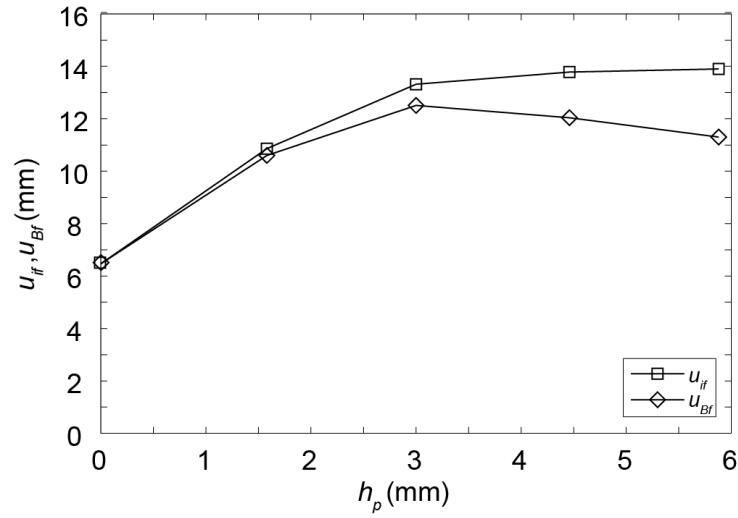
(a)



(b)



(c)



**Figure 6:**

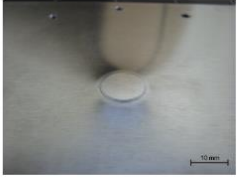


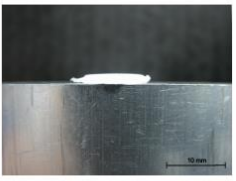
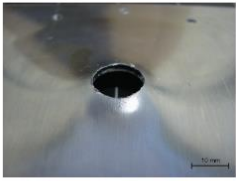
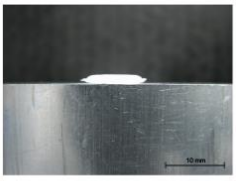
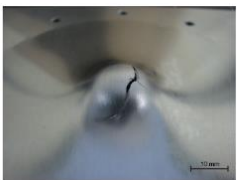
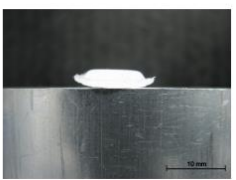
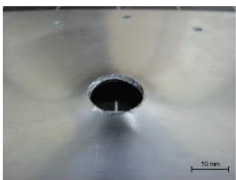
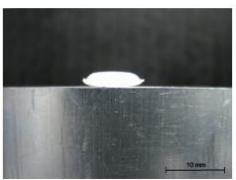
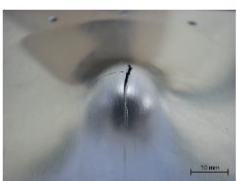
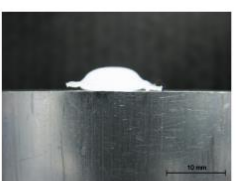

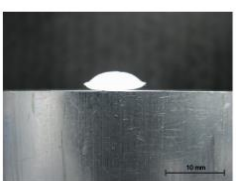
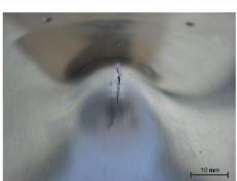
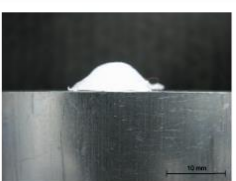

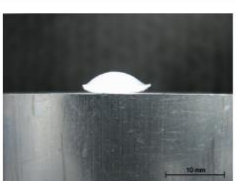
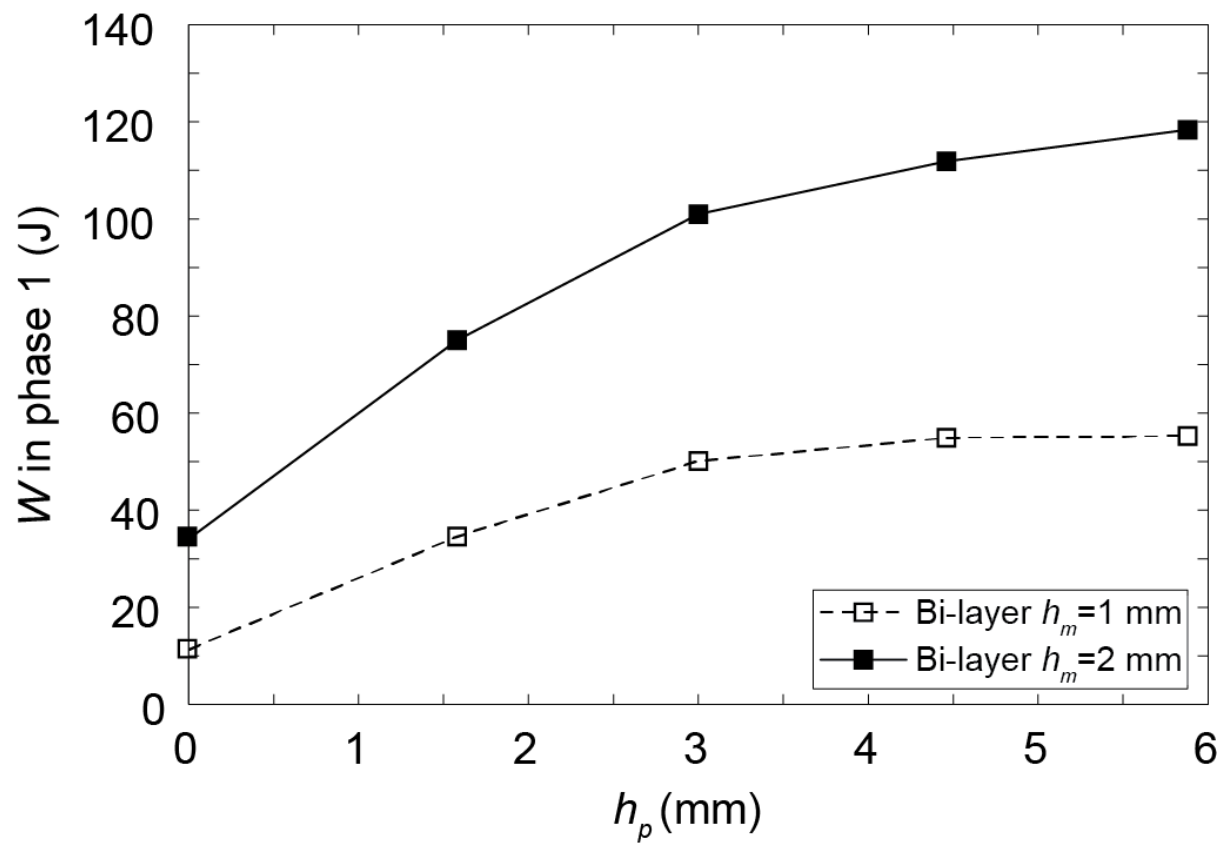
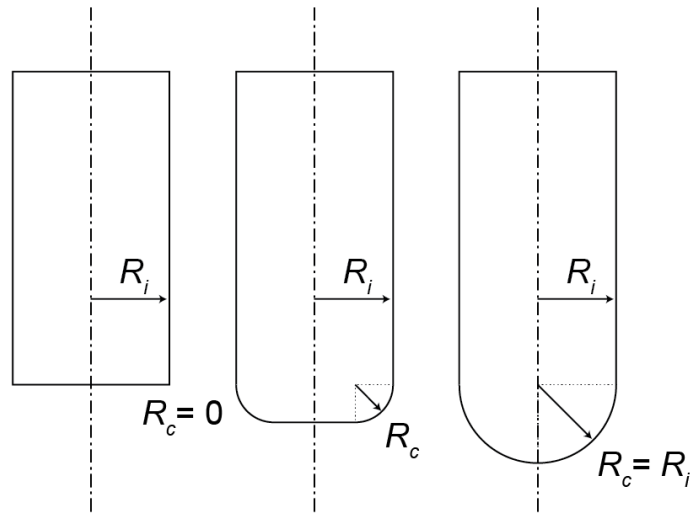
	$h_m = 1 \text{ mm}$		$h_m = 2 \text{ mm}$	
$h_p$	metal fracture	plug shape	metal fracture	plug shape
0				
1.6 mm				
3.0 mm				
4.5 mm				
5.9 mm				

Figure 7:

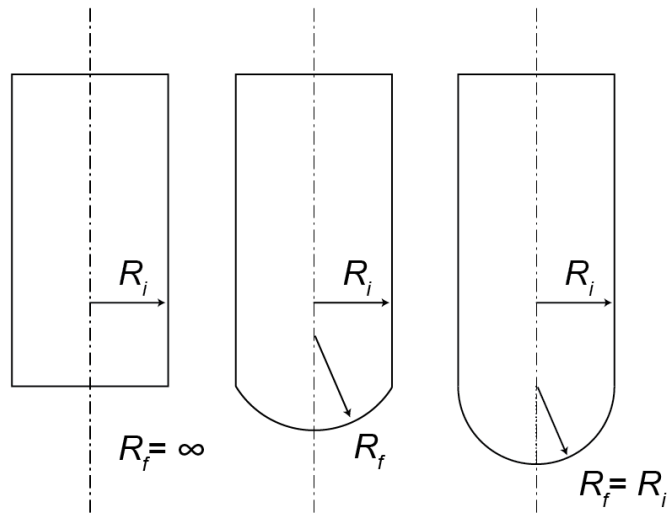


**Figure 8:**

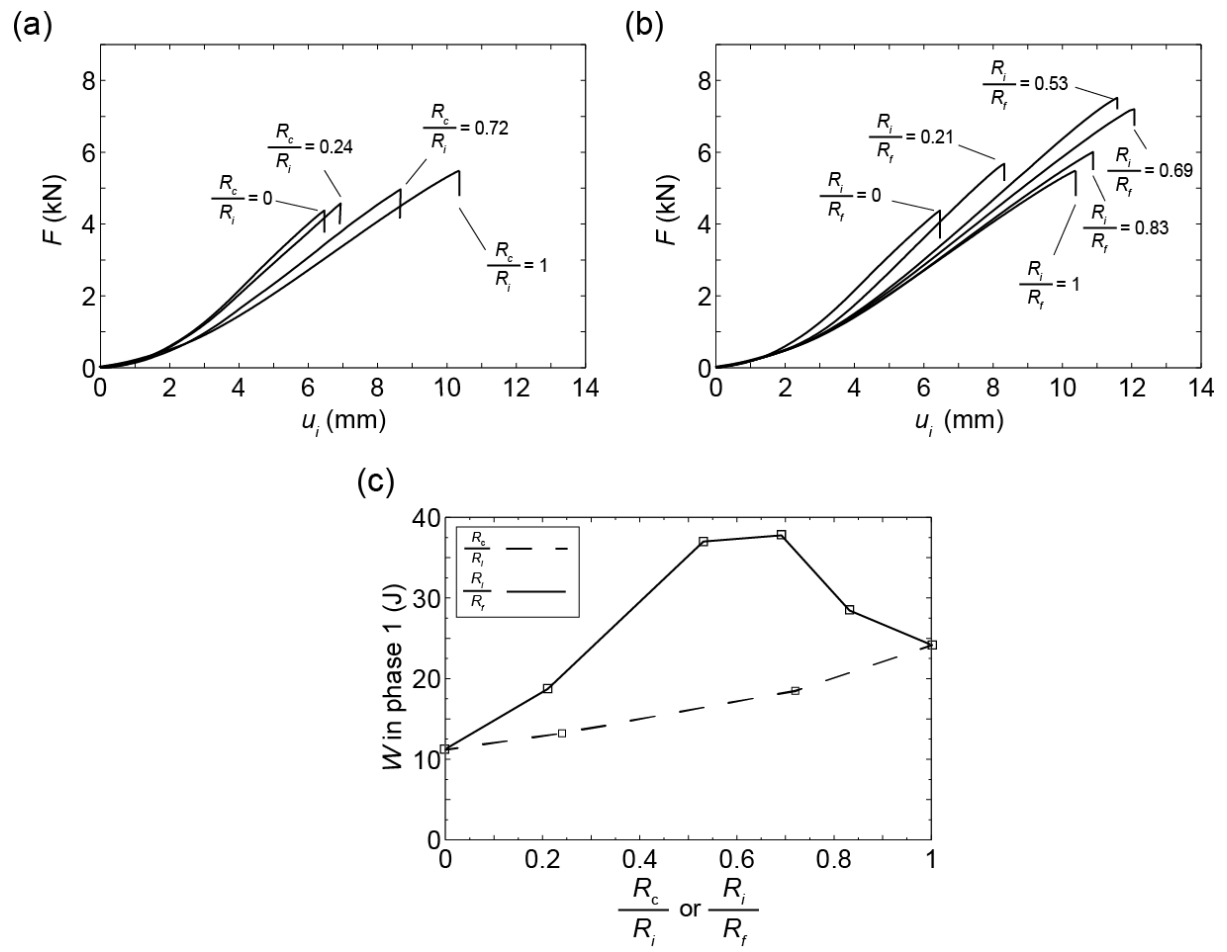
(a)



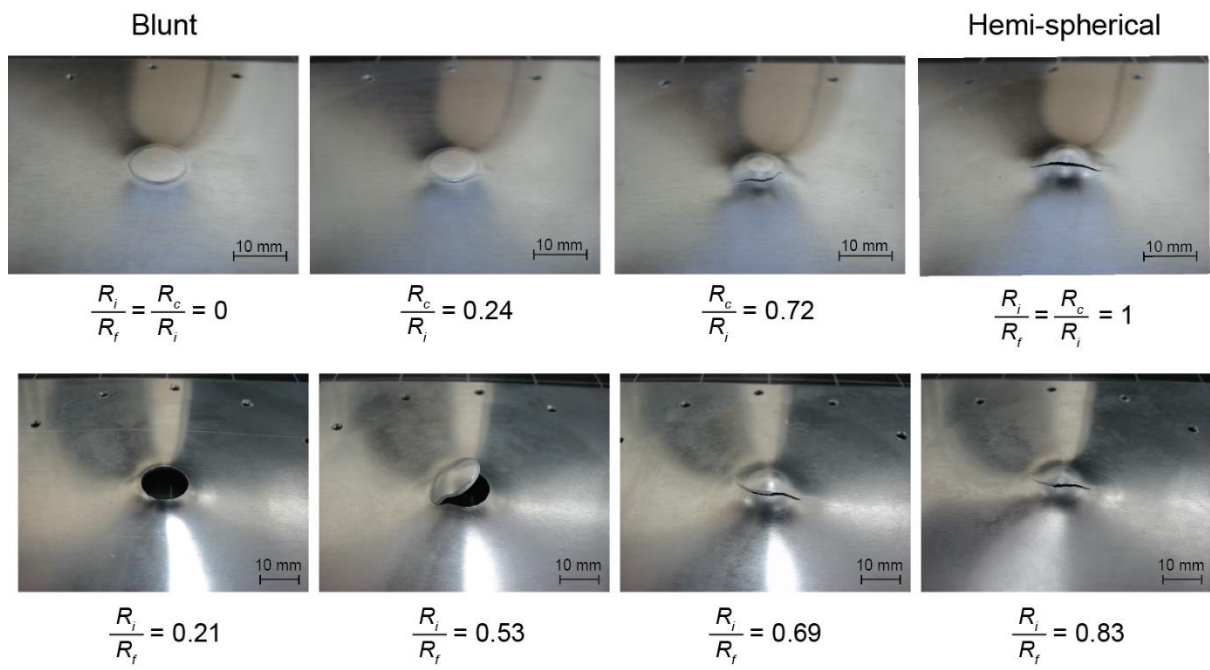
(b)



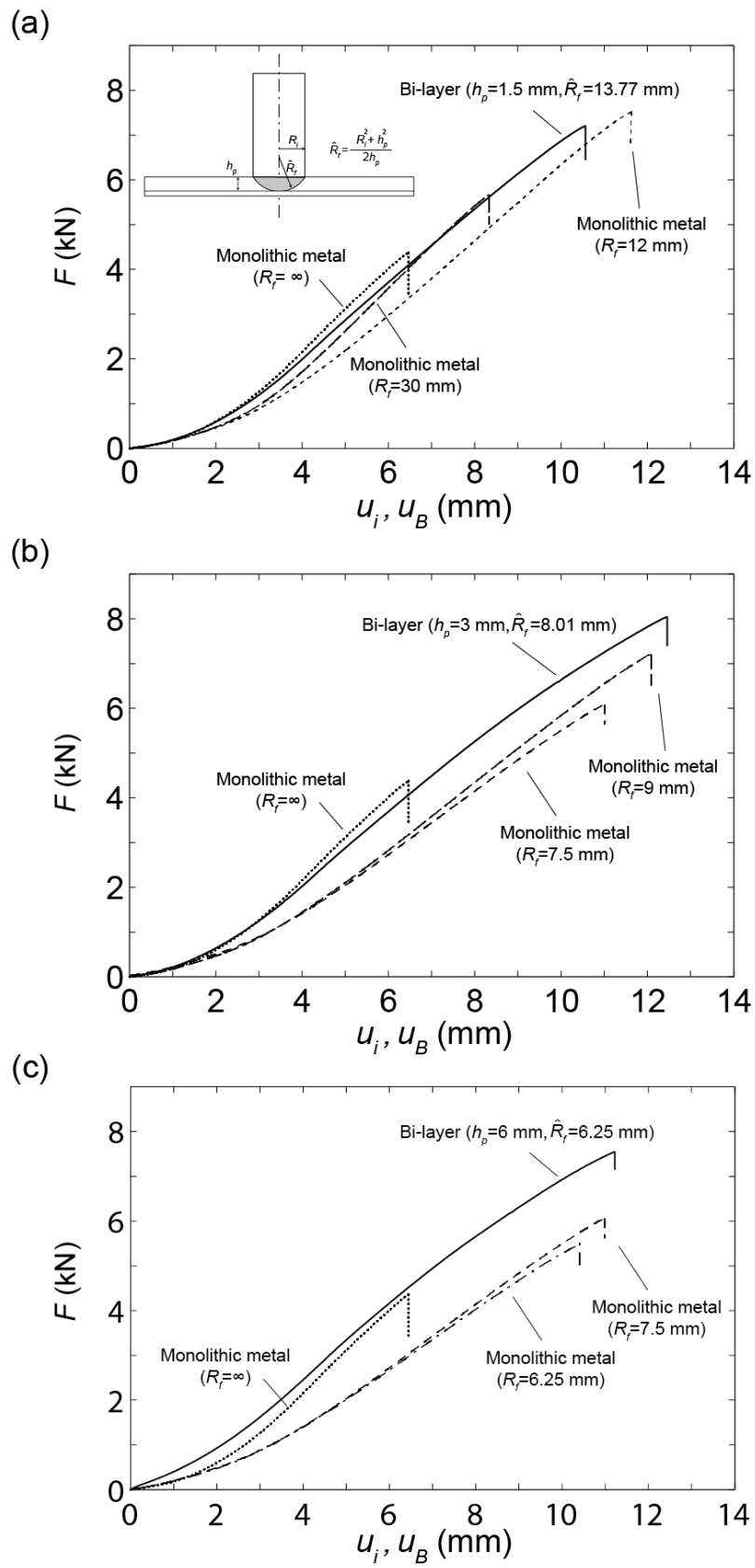
**Figure 9**



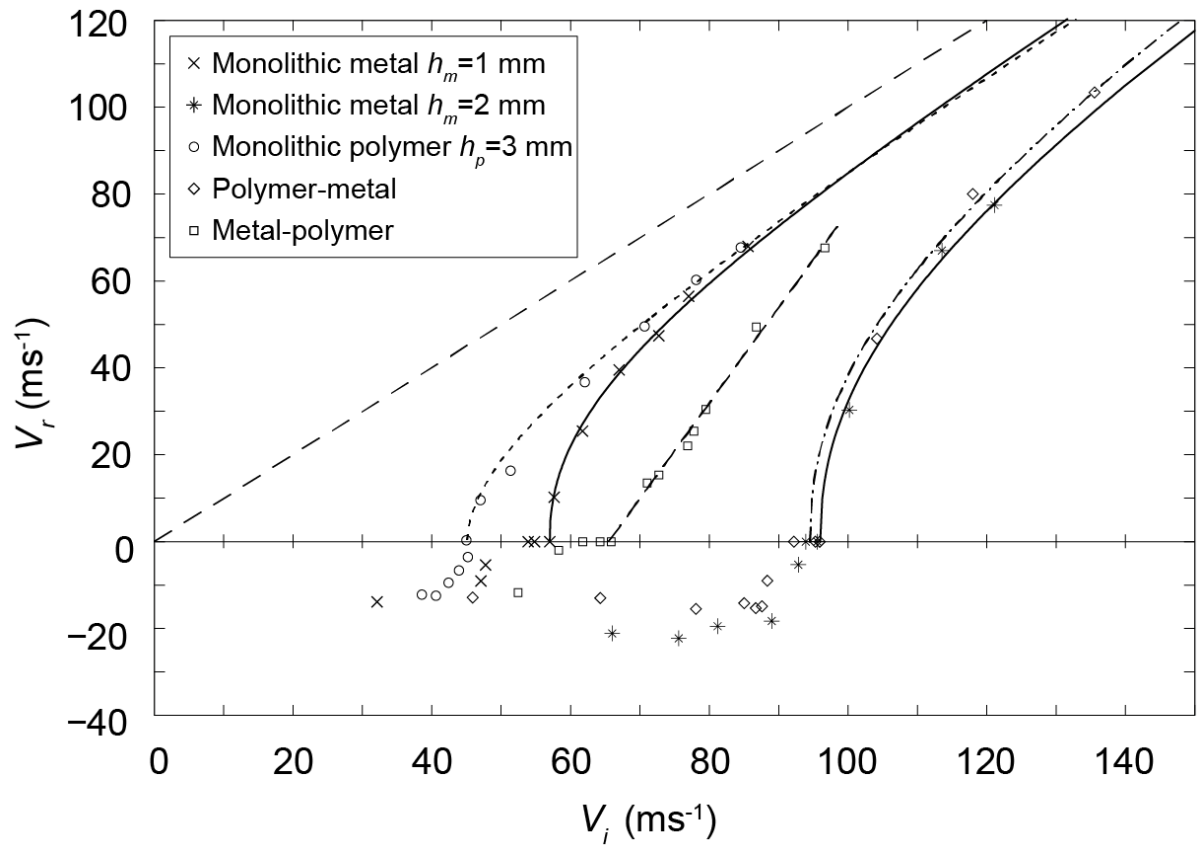
**Figure 10:**



**Figure 11:**



**Figure 12**



**Figure 13:**

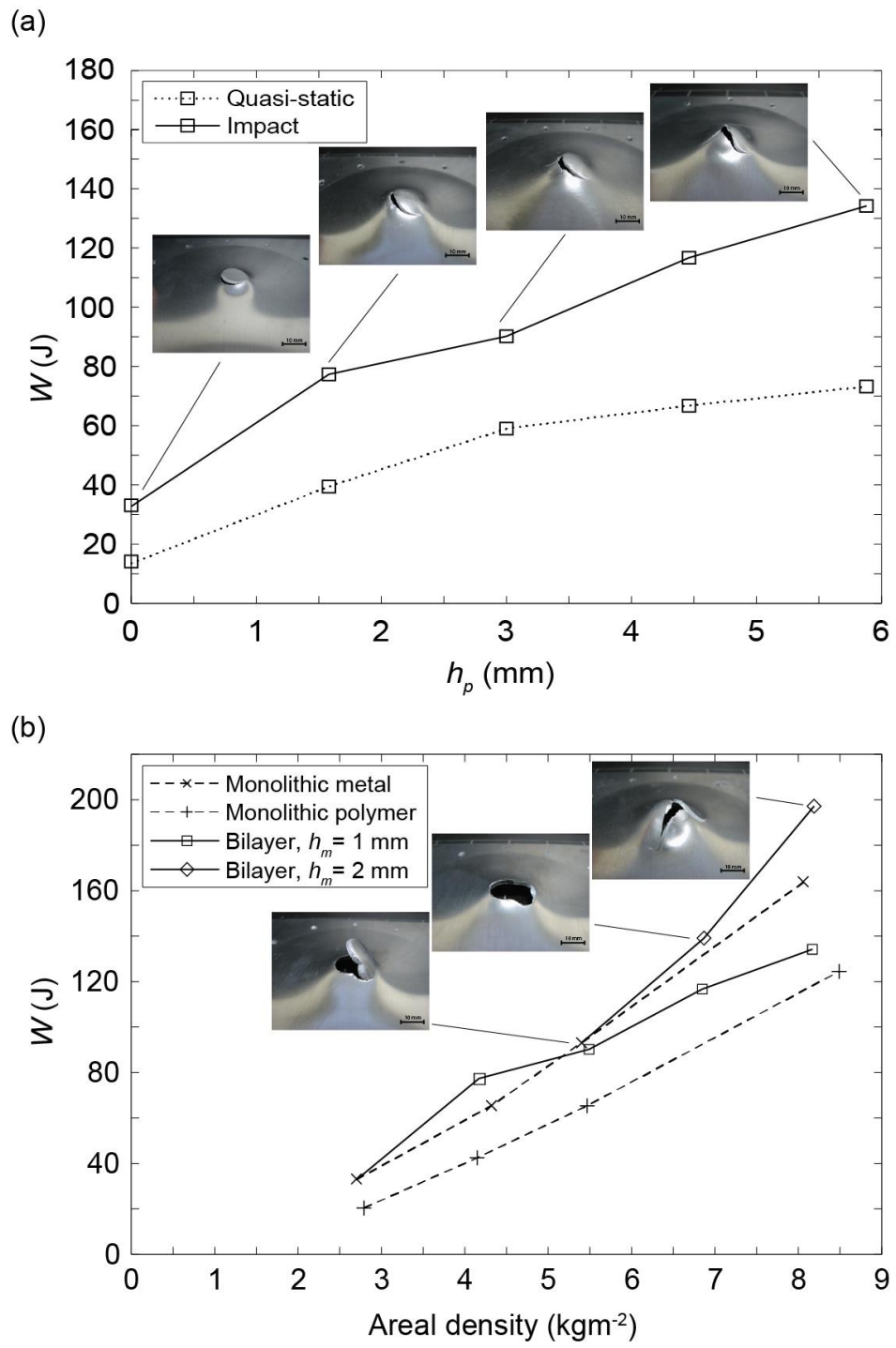
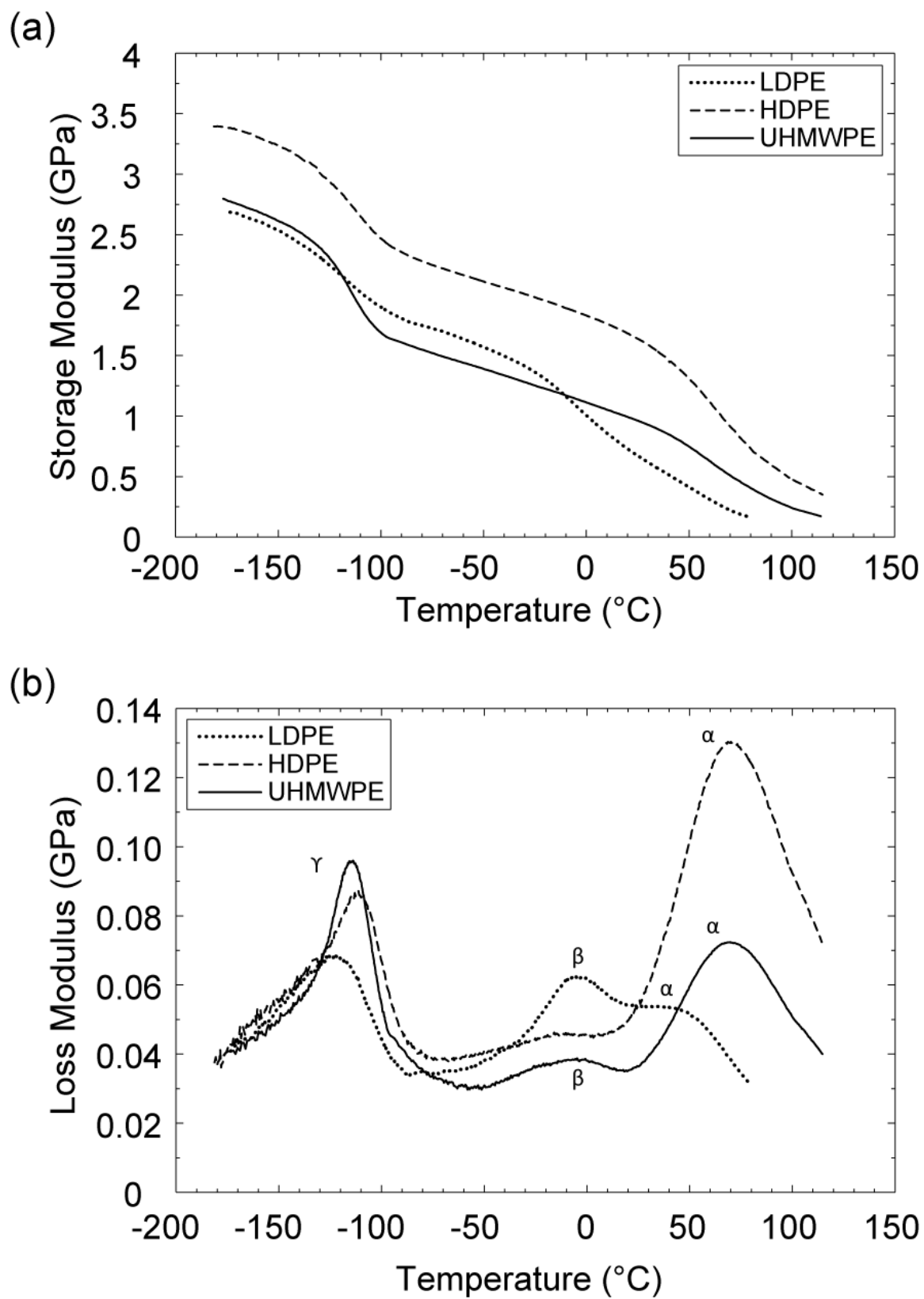
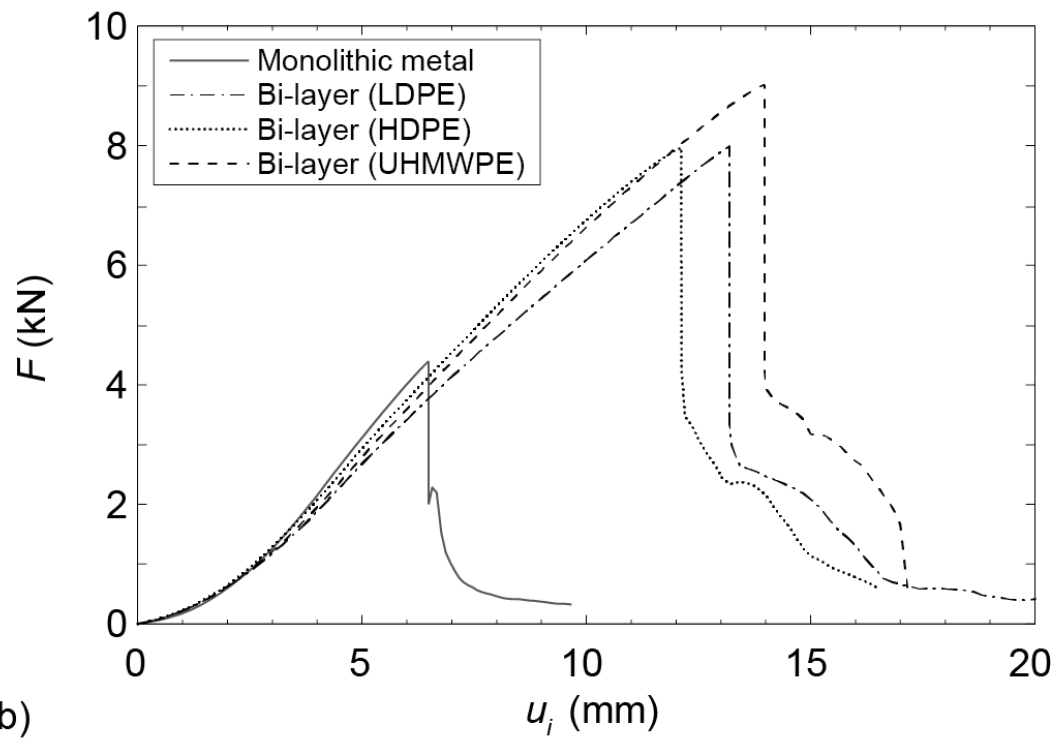


Figure 14:

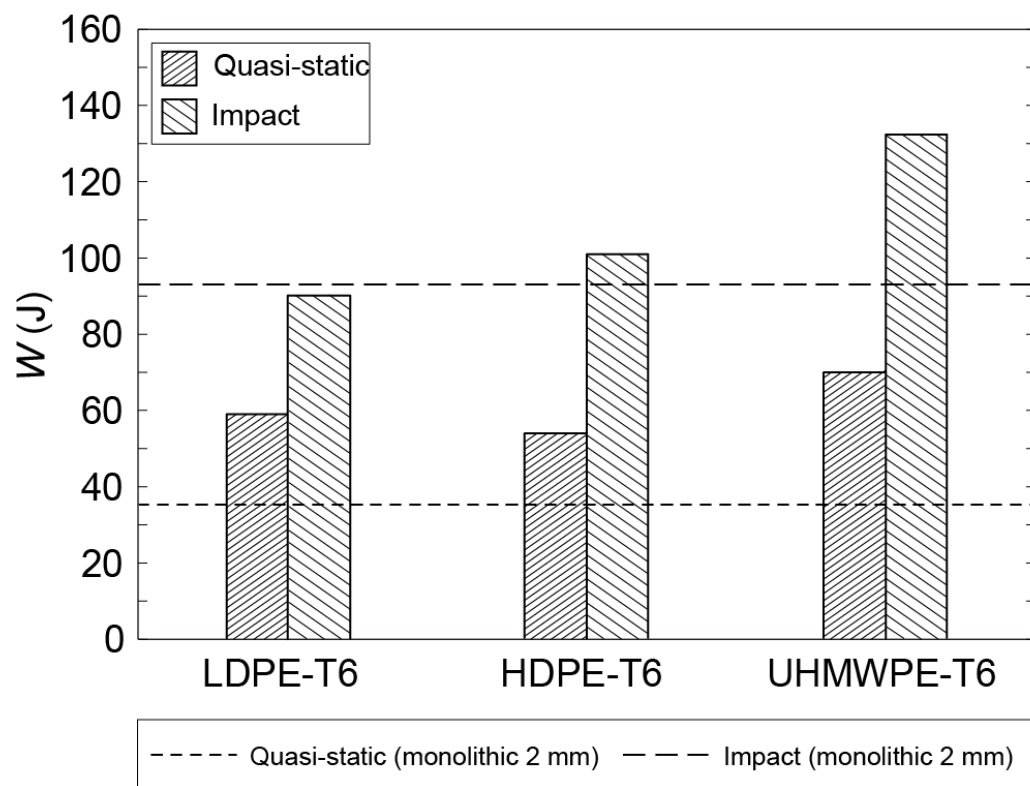


**Figure 15:**

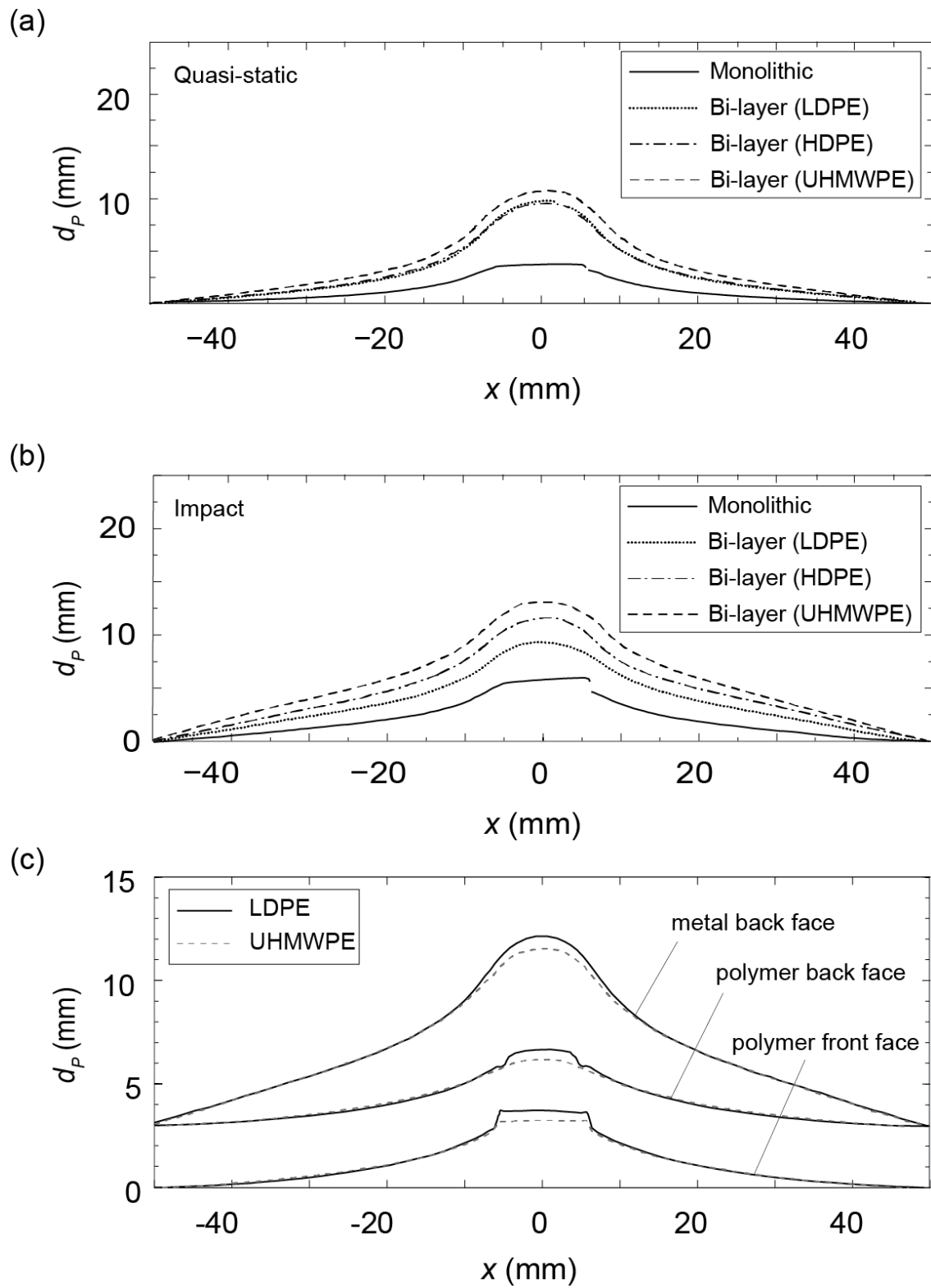
(a)



(b)



**Figure 16:**



**Table 1:**

Polymer	Strain rate (s <sup>-1</sup> )	Yield strength (MPa)	Strain at break
LDPE	0.01	11.9	7.16
	0.1	13.3	8.87
	1	16.3	2.13
HDPE	0.01	27.6	21.7
	0.1	31.3	14.0
	1	35.2	1.10
UHMWPE	0.01	22.0	10.1
	0.1	23.9	8.70
	1	26.4	6.64